

See discussions, stats, and author profiles for this publication at: <https://www.researchgate.net/publication/283846662>

# Theoretical Study of FH<sub>2</sub> – Electron Photodetachment Spectra on New Ab Initio Potential Energy Surfaces

ARTICLE in THE JOURNAL OF PHYSICAL CHEMISTRY A · NOVEMBER 2015

Impact Factor: 2.69 · DOI: 10.1021/acs.jpca.5b06153

---

READS

31

## 4 AUTHORS, INCLUDING:



Jun Chen

Dalian Institute of Chemical Physics

17 PUBLICATIONS 158 CITATIONS

[SEE PROFILE](#)



Zhigang Sun

Dalian Institute of Chemical Physics

72 PUBLICATIONS 1,059 CITATIONS

[SEE PROFILE](#)

# Theoretical Study of $\text{FH}_2^-$ Electron Photodetachment Spectra on New Ab Initio Potential Energy Surfaces

Dequan Yu,<sup>†,‡</sup> Jun Chen,<sup>†</sup> Shulin Cong,<sup>\*,†,‡</sup> and Zhigang Sun<sup>\*,†,¶</sup>

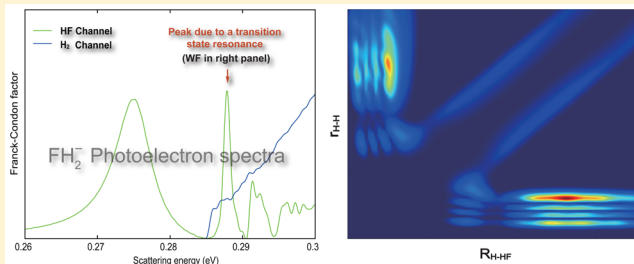
<sup>†</sup>State Key Laboratory of Molecular Reaction Dynamics and Center for Theoretical and Computational Chemistry, Dalian Institute of Chemical Physics, Chinese Academy of Sciences, Dalian 116023, People's Republic of China

<sup>‡</sup>School of Physics and Optoelectronic Technology, Dalian University of Technology, Dalian 116024, People's Republic of China

<sup>¶</sup>Center for Advanced Chemical Physics and 2011 Frontier Center for Quantum Science and Technology, University of Science and Technology of China, 96 Jinzhai Road, Hefei 230026, People's Republic of China

## Supporting Information

**ABSTRACT:** The  $\text{FH}_2^-$  anion has a stable structure that resembles a configuration in the vicinity of the transition state for neutral reaction  $\text{F} + \text{H}_2 \rightarrow \text{HF} + \text{H}$ . Electron photodetachment spectra of the  $\text{FH}_2^-$  anion reveal the neutral reaction dynamics in the critical transition-state region. Accurate quantum dynamics simulations of the photodetachment spectra using highly accurate new ab initio potential energy surfaces for both anionic and neutral  $\text{FH}_2$  are performed and compared with all available experimental results. The results provide reliable interpretations for the experimental observations of  $\text{FH}_2^-$  photoelectron detachment and reveal a detailed picture of the molecular dynamics around the transition state of the  $\text{F} + \text{H}_2$  reaction. The latest high-resolution photoelectron detachment spectra [Kim et al. *Science*, **2015**, 349, S10–S13] confirm the high accuracy of our new potential energy surface for describing the resonance-enhanced reactivity of the neutral  $\text{F} + \text{H}_2$  reaction.



## 1. INTRODUCTION

Since the first detailed studies of elementary chemical reactions at the molecular level, both experimentalists and theoreticians have attempted to probe and understand the dynamics of the critical transition state that separates reactants and products. Approximately two decades ago, Neumark and co-workers<sup>1–3</sup> developed the electron photodetachment spectroscopy technique to directly probe the molecular dynamics in the vicinity of a transition state. The stable anions of some molecules have equilibrium geometries that resemble the geometry of the transition state for a reaction involving the corresponding neutral molecule—for example,  $\text{FH}_2^-$  and the transition state for the reaction  $\text{F} + \text{H}_2 \rightarrow \text{HF} + \text{H}$ . Photoemission of an electron out of such anion therefore creates, according to the Franck–Condon principle, the neutral molecule in the vicinity of the transition state. Photodetachment spectroscopy measures the kinetic energy distribution of the ejected electron and thereby yields a resolved characteristic of vibrational structure of the neutral transition state. The combination of such experiments with quantum scattering calculations of the nucleus motion on accurate ab initio potential energy surfaces (PESs) of the neutral species and anion has resulted in a quantitative understanding of the transition-state dynamics for the  $\text{F} + \text{H}_2$  reaction.<sup>4</sup>

The reaction  $\text{F} + \text{H}_2/\text{HD}$  is one of the main prototypes of exothermic abstraction reactions. It is also a prototypical system for investigating dynamic resonances and an important system

for studying nonadiabatic reaction dynamics.<sup>5–7</sup> Since the first theoretical prediction of reaction resonances in the  $\text{F} + \text{H}_2$  reaction in the early 1970s by Schatz et al.<sup>8,9</sup> and Wu et al.,<sup>10</sup> the search for evidence of such resonances in this reaction has attracted much attention from many groups. In 1984, Neumark et al. performed a landmark crossed-beams experiment on the  $\text{F} + \text{H}_2$  reaction using a universal crossed molecular beams apparatus.<sup>11,12</sup> A clear forward scattering peak was observed for the  $\text{HF}(v' = 3)$  product, which was attributed to reaction resonances in this reaction. Furthermore, forward scattering for the  $\text{DF}(v' = 4)$  product from  $\text{F} + \text{D}_2$  as well as the  $\text{HF}(v' = 3)$  product from  $\text{F} + \text{HD}$  were observed,<sup>13</sup> consistent with the  $\text{F} + \text{H}_2$  experiment.<sup>11</sup> However, the full quantum mechanical scattering calculations of the  $\text{F} + \text{H}_2$  reaction on the Stark–Werner (SW) PES<sup>14</sup> did not support this resonance conjecture. Quasi-classical trajectory (QCT) calculations on the same surface by Aoiz et al. also exhibit forward scattering of  $\text{HF}(v' = 3)$  in the same reaction.<sup>14</sup> The SW PES is reasonably accurate in describing the transition-state region for the  $\text{F} + \text{H}_2$  reaction as revealed in the negative ion photodetachment study of the

**Special Issue:** Dynamics of Molecular Collisions XXV: Fifty Years of Chemical Reaction Dynamics

**Received:** June 26, 2015

**Revised:** October 25, 2015

$\text{FH}_2^-$  system.<sup>4</sup> Observation of forward scattered<sup>15,16</sup>  $\text{HF}(v' = 3)$  product from QCT calculations based on classical mechanics on the SW PES implies that the  $\text{HF}(v' = 3)$  forward scattering observed in the experiment might be due to mechanisms other than resonances, because resonance is a quantum phenomenon, which cannot be described properly by classical mechanics.

In a more recent crossed beam experiment, Skodje et al. unambiguously observed a step in the total excitation function at  $\sim 0.5$  kcal/mol collision energy in the  $\text{F} + \text{HD} \rightarrow \text{HF} + \text{D}$  reaction.<sup>17–20</sup> Theoretical analysis based on the SW PES attributed this step to a single reaction resonance in the  $\text{F} + \text{HD}$  reaction. Differential cross sections for this reaction measured at various collision energies also revealed a resonance signature in the reaction.<sup>21</sup> However, no step in the excitation function similar to that for the  $\text{F} + \text{HD}$  reaction was observed for the  $\text{F} + \text{H}_2$  reaction,<sup>22</sup> suggesting the dynamics for these two systems are considerably different. Theoretical study on the SW PES also found that resonance in the  $\text{F} + \text{HD}$  reaction has a profound effect on the reactive cross section at collision energies below and above the barrier and thus the reaction rate constant.

In the past few years, extensive studies on the  $\text{F} + \text{H}_2(\text{HD})$  reaction have been performed in an effort to understand the dynamics of reaction resonances, using the high-resolution crossed molecular beams technique in combination with full quantum scattering calculation based on several PESs with increasing accuracy, including Xu–Xie–Zhang (XXZ),<sup>23</sup> Fu–Xu–Zhang (FXZ),<sup>24</sup> and Chen–Sun–Zhang (CSZ)<sup>25</sup> PESs, in Yang's group.<sup>26–33</sup> A clear picture of reaction resonances has emerged for the  $\text{F} + \text{H}_2$  reaction now, in which two Feshbach resonances are important in this reaction at the low collision energies. The interference between these two Feshbach resonances plays an important role in the observed differential cross sections (DCSs) of the reactive scattering. In contrast, there is only one transition resonance state in the  $\text{F} + \text{HD}$  reaction, which is important in the low collision energy. Through the studies of the isotope-substituted  $\text{F} + \text{HD} \rightarrow \text{HF} + \text{D}$  reaction, the PES was improved and led to the FXZ PES<sup>24</sup> from the XXZ PES<sup>23</sup> with nearly spectroscopic accuracy.<sup>29,34</sup> With the accurate FXZ PES, the forward scattering  $\text{HF}(v' = 3)$  phenomenon was observed and attributed largely to a slow-down mechanism over the exit barrier in the  $\text{F} + \text{H}_2$  reaction.<sup>30</sup> The shape resonance mechanism only plays a minor role in a narrow range of collision energy. The effect of the  $\text{H}_2$  reagent rotational excitation on the reaction resonances in the  $\text{F} + \text{H}_2$  reactions has also been investigated.<sup>27</sup> Both experimental and theoretical results show that reagent rotational excitation has a profound effect on the dynamics of the resonance-mediated reaction. In 2010, a relevant progress on detecting the reactive resonances in the  $\text{F} + \text{H}_2$  reaction and its isotopic analogues is the observation of the partial wave resonance in the  $\text{F} + \text{HD}$  reaction in Yang's group, which is the finest structure observed in a chemical reaction with collision energy of  $\sim 1.0$  kcal/mol.<sup>31</sup> Because of the efficient resonance-enhanced tunneling, it is found that even with a reaction barrier of  $\sim 1.67$  kcal/mol,<sup>35</sup> the reaction rate constant of  $\text{F} + \text{H}_2$  at interstellar temperature ( $\sim 2\text{--}3$  K) is still considerable.<sup>36</sup> Through the detailed investigations, an accurate physical picture of reaction resonances in this benchmark reaction has been established, providing an excellent case of dynamical resonances in elementary chemical reactions.

Besides the work mentioned above, using the lifetime matrix analysis, De Fazio and their co-workers calculated the time

delay of the resonance states in the reaction of  $\text{F} + \text{HD}/\text{H}_2$ .<sup>37–39</sup> Sokolovski and his co-workers applied the complex angular momentum analysis with the help of Páde approximation for the S-matrix of the reaction of  $\text{F} + \text{H}_2$ , and Regge poles were identified.<sup>40,41</sup> The role of the van der Waals well in the reactant channel in the branching ratio of the  $\text{F} + \text{HD}$  reaction at low collision energy,<sup>42–48</sup> and the role of the spin-orbit effects<sup>5,7,49</sup> in the reaction  $\text{F} + \text{H}_2/\text{D}_2/\text{HD}$  reaction, have received extensive studies also.

Recently, Wang et al.<sup>50</sup> observed reactive resonance in the vibrationally excited  $\text{HD}(v = 1) + \text{F} \rightarrow \text{HF} + \text{D}$  reaction by a full quantum state-resolved crossed molecular beam apparatus. To more accurately describe the vibrationally excited  $\text{HD}(v = 1) + \text{F} \rightarrow \text{HF} + \text{D}$  reaction, the FXZ PES<sup>24</sup> for the reaction system was improved by adding higher-level ab initio data points around the transition barrier, where the PES requests more elaborate treatment. Extensive studies showed that the new CSZ PES,<sup>25</sup> without any scaling factor to the original ab initio energies, is better than the FXZ PES in describing the various dynamic processes in the  $\text{FH}_2/\text{HD}$  system,<sup>50</sup> even both of them are capable of predicting the experimental observations very well.<sup>34</sup>

The features of the transition state of a reaction are very difficult to measure directly with any current experimental techniques, except the negative ion photodetachment spectroscopy put forward by Neumark and his co-workers.<sup>4</sup> To characterize the structure of the transition state of the  $\text{F} + \text{H}_2$  reaction and thereby shed light on the nature of the chemical bonds that break and form during a chemical reaction, the photodetachment spectroscopies for  $\text{FH}_2^-$  were measured by Neumark and co-workers in the past decades.<sup>4,51–54</sup> Several quantum time-dependent wavepacket simulations of the  $\text{FH}_2^-$  photodetachment spectra on different ab initio PESs have also been performed,<sup>53,55–58</sup> including the T5a PES,<sup>59</sup> the M5 PES,<sup>60</sup> the TS PES,<sup>61</sup> the SSEC PES,<sup>62</sup> the SW PES,<sup>63</sup> and the HSW PES.<sup>58</sup> In a recent important paper,<sup>54</sup> the Berkeley group reported a set of high-resolution photodetachment spectra for para- $\text{FH}_2^-$  and normal- $\text{FH}_2^-$  using slow electron velocity-map imaging technique. Two narrow peaks were found at roughly the same electronic binding energy in the para- $\text{FH}_2^-$  and normal- $\text{FH}_2^-$  spectra.

Very recently, Kim et al.<sup>64</sup> reported electron photodetachment spectroscopies with unprecedented high resolution using cooled anion precursors, and several narrow peaks not seen in previous experiments were observed. On the basis of a highly accurate  $\text{F} + \text{H}_2$  Li–Werner–Alexander–Lique (LWAL) PES,<sup>6,49</sup> these peaks were assigned to resonances associated with quasibound states in the  $\text{HF} + \text{H}$  and  $\text{DF} + \text{D}$  product arrangements and with a quasibound state in the transition-state region of the  $\text{F} + \text{H}_2$  reaction. With experimentally determined electron affinity of  $\text{F}$  atom ( $\text{EA}(\text{F}) = 3.4012$  eV),<sup>65</sup> and theoretically determined dissociation energy  $D_0$  of  $\text{FH}_2^-$ , which is 0.2005 eV for  $\text{FH}_2^-$  and 0.2219 eV for  $\text{FD}_2^-$  obtained on new ab initio PES at CCSD(T)-F12a<sup>66,67</sup> level, Kim et al. argued that the LWAL is the most accurate one among all available PESs for neutral  $\text{F} + \text{H}_2$  for reproducing the high-resolution electron photodetachment spectra, since the energy position of the peak *a* due to the (3, 0, 1) (in their assignment, as (3, 0, 0), *vide infra*) resonance state can be accurately reproduced. To do that, they found that the adopted  $D_0$  of  $\text{FH}_2^-$  does not require any scaling factor, and  $\text{EA}(\text{F})$  is directly taken from accurate experiment.

Since the FXZ and CSZ PESs have been proven being accurate for describing the reactive scattering process of  $F + H_2$  and  $F + HD$ ,<sup>25,34</sup> it is surprising that they are unable to accurately reproduce the fine peaks observed in the high-resolution photodetachment spectra. At the same time, it would be interesting to investigate in detail the performances of different PESs on reproducing the photodetachment spectra and their implications to the reactive resonances observed in a molecular crossed beam experiment.

In this paper, we present a detailed quantum mechanical study of the  $FH_2^-$  photodetachment spectroscopy. For the neutral  $F + H_2$ , the CSZ PESs are mainly applied. The dynamics calculations are also performed with the LWAL, FXZ, and SW PES for comparison. For the negative ion  $FH_2^-$ , a newly constructed PES using ab initio method at currently highest level are constructed and applied in the calculations. In contrast to the study by Kim et al.,<sup>64</sup> we found that the calculated photodetachment spectra using the FXZ and CSZ PESs are in excellent agreement with the high-resolution experimental data,<sup>54,64</sup> and a detailed assignment of the spectrum characteristics is presented. The reason is that we found that it is very difficult to give the value of  $D_0$  of  $FH_2^-$  with accuracy of less than 2 meV, if not impossible, using current state-of-art ab initio method. At the same time, the rovibrational state distribution of the photofragments is given to get a full insight into the  $F + H_2$  dynamics. Combined with the crossed molecular beam experiment, instead on the ground of the accuracy of the value of  $D_0$  of  $FH_2^-$ , we finally conclude that the FXZ or CSZ PES indeed be the most accurate PES currently, consistent with our previous studies.

This paper is organized as follows: In Section 2 the basic theory and some computational details for simulating the photodetachment spectra are presented. Section 3 presents the numerical results and the comparison with the experimental spectra. In Section 4 we summarize our conclusions. Atomic units are used throughout the paper unless otherwise stated.

## 2. COMPUTATIONAL DETAILS

**2.1. Theoretical Methods for Simulating the  $FH_2^-$  Photodetachment Spectroscopy.** In the calculations of the  $FH_2^-$  photodetachment spectra, as Russell et al. had done,<sup>57</sup> we assume that the  $FH_2^-$  is sufficiently rotationally cold and can be modeled by total angular momentum  $J_{\text{tot}} = 0$  and that the electric dipole transition matrix element for the electronic transition varies rather slowly with the nuclear coordinates in the Franck–Condon region and with the kinetic energy of the ejected photodetachment.<sup>68</sup> With these two assumptions, the photodetachment spectra can be simulated by using the Franck–Condon factors<sup>55</sup> according with the following two different formalisms.

The Franck–Condon factor can be evaluated, in the first formalism, by the Fourier transformation of the autocorrelation function (FTA), following the work of Manolopoulos:<sup>57</sup>

$$P(E) = \text{Re} \left[ \frac{1}{\pi\hbar} \int_0^\infty e^{iEt/\hbar} C(t) dt \right] \quad (1)$$

where the autocorrelation function can be written as

$$C(t) = \langle \phi_i | e^{-iHt/\hbar} | \phi_i \rangle \quad (2)$$

Here,  $|\phi_i\rangle$  is the initial rovibrational state of  $FH_2^-$ ,  $H$  is the Hamiltonian of  $FH_2$ , and  $E$  is the scattering energy measured relative to the classical bottom of the  $F + H_2$  asymptote.

In the second formalism, the Franck–Condon factor can also be calculated using the flux formalism (FF).<sup>55,69,70</sup> As in the photodetachment emission process, an initial rovibrational state of  $FH_2^-$ ,  $|\phi_i\rangle$ , evolves into a scattering wave function on the dissociative PES of  $FH_2$ , which can be regarded as a usual photodissociation process. The scattering wave with energy  $E$  may be decomposed into components,  $|\Psi_{\lambda j}(E)\rangle$ . Here the arrangement channel is specified by  $\lambda$ , and the vibration/rotation quantum number associated with each channel is specified by  $v/j$ . The Franck–Condon factor associated with the photoproduct state ( $v, j$ ) in channel  $\lambda$  can be simply calculated by

$$P_{\lambda vj-i}(E) = |\langle \Psi_{\lambda vj}(E) | \phi_i \rangle|^2 \quad (3)$$

The total photodetachment spectrum is the sum of eq 3 over all the energetically allowed final states

$$P(E) = \sum_{\lambda vj} P_{\lambda vj-i}(E) \quad (4)$$

The contribution from each final state,  $P_{\lambda vj-i}$ , can be calculated using the time-dependent wavepacket method.<sup>70</sup> In this method, the time-independent components of the initial state with scattering energy  $E$  can be calculated via the Fourier transformation of the time-dependent wavepacket:

$$|\Phi_i(E)\rangle = \int_0^\infty dt e^{i(E-H)t/\hbar} |\phi_i\rangle \quad (5)$$

In the reactant or product asymptotic region at the analysis plane  $R = R_L^\lambda$ , the time-independent component  $|\Phi_i(E)\rangle$  can be expanded in terms of the basis function  $|\psi_{\lambda vj}\rangle$  of the associated channel

$$|\Phi_i(E)\rangle = \sum_{\lambda vj} A_{\lambda vj-i}(E, R_L^\lambda) |\psi_{\lambda vj}\rangle \quad (6)$$

The contribution of final rovibrational states ( $v, j$ ) to the total photodetachment spectrum at scattering energy  $E$ ,  $P_{\lambda vj-i}$ , can be obtained from the expansion

$$P_{\lambda vj-i}(E) = \text{Im} \left[ \frac{\hbar^2}{2\pi\mu_R} \left[ A_{\lambda vj-i}^* \frac{d}{dR} A_{\lambda vj-i} \right]_{R=R_L^\lambda} \right] \quad (7)$$

where  $\mu_R$  is the reduced mass for the reaction coordinate  $R$ .

Both of the two formalisms can offer a reliable interpretation for the experimental photodetachment spectra but from different aspects, assuming the total propagation time is long enough. In the present work, they are both adopted to provide a comprehensive interpretation of the photodetachment spectra and reveal the mechanism of the reaction dynamics. We will find that the numerical results calculated by the two methods are consistent with each other. However, for the photodetachment involving intermediate states of extremely long lifetime, the second FF method is more difficult to obtain converged results with respect to total propagation time, since those states will reside in the interaction region long time and it is difficult to fully collect its flux at the asymptotic region. However, the FF method is capable of giving photodetachment fragments information, unlike the FTA method that provides only the spectra with an uniform artificial lifetime for all peaks. Thus, the FF method is helpful for understanding the underlying molecular dynamics of the structure of the spectra.

Both the FTA and FF methods require the time-dependent wavepacket calculation on the neutral  $FH_2$  PES in our present

work. In the Jacobi coordinates of the F + H<sub>2</sub> arrangement, the Hamiltonian for a given total angular momentum  $J_{\text{tot}}$  can be written as<sup>71</sup>

$$H = -\frac{\hbar}{2\mu_R} \frac{\partial^2}{\partial R^2} - \frac{\hbar}{2\mu_r} \frac{\partial^2}{\partial r^2} + \frac{(J_{\text{tot}} - j)^2}{2\mu_R R^2} + \frac{j^2}{2\mu_r r^2} + V \quad (8)$$

where  $R$  is the distance from F to the center of mass of H<sub>2</sub>,  $r$  is the bond distance of H<sub>2</sub>,  $J_{\text{tot}}$  is the total angular momentum operator, and  $j$  is the rotational angular momentum operator of H<sub>2</sub>.  $\mu_r$  is the reduced mass of H<sub>2</sub>, and  $V$  is the PES for neutral F + H<sub>2</sub> system. The Hamiltonian is represented using the Sinc-DVR<sup>72</sup> for the radial coordinates  $R$  and  $r$  and Legendre polynomial basis functions for the angular coordinate. To avoid the wave packet reflecting back from the boundaries, especially when moving slowly, an absorbing potential is employed with the same form as in our previous work in a long grid range.<sup>73</sup> The numerical parameters applied in the time-dependent wavepacket calculations are listed in Table 1. It is observed that,

**Table 1. Numerical Parameters in the Time-Dependent Wavepacket Calculations (all in atomic unit, except specified)**

| F + H <sub>2</sub>                |  |
|-----------------------------------|--|
| grid/basis range and size         | $R [0.1, 50.0]$ , $N_R = 531$  |
| absorbing potential <sup>73</sup> | $r [0.6, 50.0]$ , $N_r = 383$  |
| $n' = 2$                          | $j_{\min} = 0$ , $j_{\max} = 362$ , $N_j = 363$<br>$C'_a = 0.0006$ , $C'_b = 0.005$ , $R_a = 18.0$ ,<br>$R_b = 48.0$ |
| $n = 1$                           | $C_a = 0.001$ , $C_b = 0.06$ , $r_a = 30.0$ ,<br>$r_b = 48.0$  |
| propagation                       | time step:<br>$\Delta t = 4$ au<br>total time: 120 K au  |

to obtain accurate numerical results for the wave packet propagation on the PES of neutral FH<sub>2</sub>, the grid range must be huge, and high-quality absorbing potentials are necessary.

**2.2. Potential Energy Surfaces.** To calculate the photodetachment spectra of FH<sub>2</sub><sup>-</sup>, we first need to calculate the initial state from the PES for FH<sub>2</sub><sup>-</sup>, then propagate the initial rovibrational state wave function of FH<sub>2</sub><sup>-</sup> on the neutral FH<sub>2</sub> PES. In refs 4 and 57, a harmonic approximation,<sup>55</sup> using the equilibrium geometry and normal-mode frequencies from the ab initio calculations of Simons and co-workers,<sup>74</sup> was used to describe the rovibrational states of FH<sub>2</sub><sup>-</sup>, and the time-dependent wavepacket calculations were performed on the SW PES.<sup>63</sup> In ref 58, the initial state was calculated on a new ab initio PES for anion (hereafter SWA), and a new spin-orbit corrected PES for neutral FH<sub>2</sub> (hereafter HSW) based on the SW PES was used for solving and propagating the FH<sub>2</sub><sup>-</sup> rovibrational state wave function.

In the present work, our calculations are performed on highly accurate ab initio PESs for both anionic and neutral FH<sub>2</sub>. The applied CSZ PES for neutral FH<sub>2</sub> was recently reported<sup>50</sup> and has been proven rather accurate in describing various dynamic processes in the FH<sub>2</sub> system. For calculating the initial rovibrational state of FH<sub>2</sub><sup>-</sup>, we construct a highly accurate PES for the anion (hereafter YCS) by using the hierarchical construction method.<sup>24</sup> Briefly, the YCS PES is constructed by the neutral network method<sup>76</sup> with ab initio calculations of the electronic energies at a relatively high level of theory, based

upon 3205 energy points calculated using the UCCSD(T)/aug-cc-pvSZ method and 804 energy points calculated using the UCCSD(T)/aug-cc-pv6Z method with energies under 4 eV. All of the ab initio calculations were performed using Molpro program.<sup>75</sup>

Since the shape of the PES of the FH<sub>2</sub><sup>-</sup> calculated by the ab initio method at higher level than UCCSD(T)/aug-cc-pvSZ does not change much, especially around equilibrium geometry, to evaluate the role of the effect of higher excitation and the role of the relativistic effect in determination the accuracy of the value of  $D_0$  of FH<sub>2</sub><sup>-</sup>, the CCSDT(2)<sub>Q</sub> method and multi-reference configuration interaction (MRCI) method were also applied to calculate the energy of FH<sub>2</sub><sup>-</sup> at the geometry of bottom of FH<sub>2</sub><sup>-</sup> well and asymptotic region of F<sup>-</sup> + H<sub>2</sub>.

For a comparison, the electron photodetachment spectra calculated for neutral FH<sub>2</sub> using the SW PES, LWAL PES, and FXZ PES are also calculated and presented.

### 3. RESULTS AND DISCUSSION

#### 3.1. Vibrational States of the YCS Potential Energy Surface.

The vibrational states of anion FH<sub>2</sub><sup>-</sup> for  $J_{\text{tot}} = 0$  are obtained by diagonalizing the Hamiltonian in the F<sup>-</sup>+H<sub>2</sub> Jacobi coordinates using the Lanczos method. The eigenenergies for the first six bound states of FH<sub>2</sub><sup>-</sup> on both SWA PES<sup>58</sup> and YCS PES are listed in Table 2. The weakly bound states of FH<sub>2</sub><sup>-</sup>

**Table 2. Comparison of the first six eigenenergies of FH<sub>2</sub><sup>-</sup> on the present YCS PES and SWA PES<sup>b</sup>**

| No. | $E^a$ (cm <sup>-1</sup> ) |                     | symmetry <sup>d</sup>              |
|-----|---------------------------|---------------------|------------------------------------|
|     | SWA-PES <sup>b</sup>      | YS-PES <sup>c</sup> |                                    |
| 1   | 598.51                    | 558.29              | para-FH <sub>2</sub> <sup>-</sup>  |
| 2   | 598.55                    | 558.33              | ortho-FH <sub>2</sub> <sup>-</sup> |
| 3   | 931.68                    | 889.76              | para-FH <sub>2</sub> <sup>-</sup>  |
| 4   | 931.94                    | 889.97              | ortho-FH <sub>2</sub> <sup>-</sup> |
| 5   | 1210.00                   | 1177.65             | para-FH <sub>2</sub> <sup>-</sup>  |
| 6   | 1210.84                   | 1178.33             | ortho-FH <sub>2</sub> <sup>-</sup> |

<sup>a</sup>Relative to the classical bottom of the F<sup>-</sup>+H<sub>2</sub> asymptote. <sup>b</sup>Numerical results of Bernd Hartke and co-workers on the SWA PES (ref 58).

<sup>c</sup>Numerical results on the YCS PES. <sup>d</sup>The nuclear spin state of H<sub>2</sub> in the FH<sub>2</sub><sup>-</sup> complex (see the text).

anion in Table 2 can be classified into two classes, para-FH<sub>2</sub><sup>-</sup> and ortho-FH<sub>2</sub><sup>-</sup>, depending on the nuclear spin state of H<sub>2</sub>. The para-FH<sub>2</sub><sup>-</sup> contains a para-H<sub>2</sub> moiety, and the ortho-FH<sub>2</sub><sup>-</sup> contains an ortho-H<sub>2</sub> moiety.

The photodetachment of these two forms of FH<sub>2</sub><sup>-</sup> accesses two distinct sets of scattering states in the neutral F + H<sub>2</sub> system. Specifically speaking, the para-FH<sub>2</sub><sup>-</sup> will lead to dissociation with product of the F + H<sub>2</sub> ( $j = \text{even}$ ) states, but the ortho-FH<sub>2</sub><sup>-</sup> will lead to dissociation with product of the F + H<sub>2</sub> ( $j = \text{odd}$ ).<sup>53</sup> Since the equilibrium geometry of FH<sub>2</sub><sup>-</sup> is linear, the eigenenergies of each pair of para- and ortho-FH<sub>2</sub><sup>-</sup> are degenerate as shown in Table 2. A comparison between the two sets of eigenenergies shows that all the first six eigenenergies obtained on the YCS PES are ~40 cm<sup>-1</sup> lower than those on the SWA PES. This results from the energy difference between the two anion PESs at the F<sup>-</sup> + H<sub>2</sub> asymptotic region. Figure 1 shows a schematic representation of the initial conditions for the nuclear dynamics of the photodetachment process, where the square modulus of the nuclear wave function for the ground rovibrational state of FH<sub>2</sub><sup>-</sup> is projected as a contour plot on the CSZ PES for the neutral

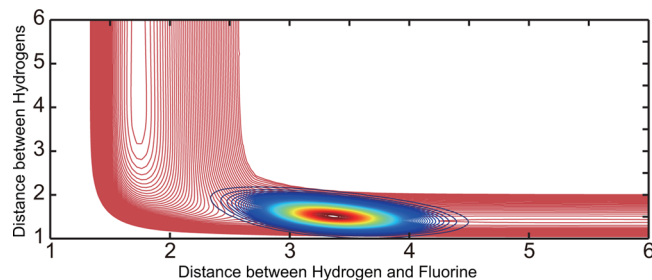


**Figure 1.** Contour plot of the F–H<sub>2</sub> PES (collinear geometry) with the FH<sub>2</sub><sup>−</sup> ground-state wave function shaded.

FH<sub>2</sub>. There is a considerable overlap between the Franck–Condon region and the transition-state region, although most of the Franck–Condon region lies in the F + H<sub>2</sub> valley.

Table 3 lists the equilibrium geometry of the YCS PES for anion, its zero-point energy, and the zero-point corrected

**Table 3. Properties of the FH<sub>2</sub><sup>−</sup> Anion**

| calculation                | <i>r</i> <sub>e</sub> (FH) <sup>a</sup> | <i>r</i> <sub>e</sub> (HH) <sup>a</sup> | ZPE <sup>b</sup> | <i>D</i> <sub>0</sub> <sup>c</sup> |
|----------------------------|---|---|------------------|------------------------------------|
| Simons et al. <sup>d</sup> | 3.194                                   | 1.455                                   | 2990             | 0.204                              |
| Stark <sup>e</sup>         | 3.290                                   | 1.482                                   | 2997             | 0.1950                             |
| Kim et al. <sup>f</sup>    | 3.302                                   | 1.480                                   | 2831             | 0.2005                             |
| present                    | 3.292                                   | 1.480                                   | 2844             | 0.2009                             |

<sup>a</sup>Bond distance in bohr. The ground state of FH<sub>2</sub><sup>−</sup> has linear structure with a terminal F atom. <sup>b</sup>Zero-point energy in inverse centimeters.

<sup>c</sup>Dissociation energy in electronvolts, see more in Supporting Information. <sup>d</sup>Reference 74. <sup>e</sup>Reference 58. <sup>f</sup>Reference 64.

dissociation energy [FH<sub>2</sub><sup>−</sup>(000) → F<sup>−</sup> + H<sub>2</sub>(*v* = 0, *j* = 0)]. We compare with values from the earlier calculations of Simons and co-workers<sup>74</sup> those by Hartke and Werner<sup>58</sup> and those by Kim et al.<sup>64</sup>

**3.2. Dissociation Energy *D*<sub>0</sub> of FH<sub>2</sub><sup>−</sup>.** The relation between the experimentally measured binding energy of the electron (eBE) and the scattering energy *E* in the theoretical simulation, which is relative to the bottom of the F + H<sub>2</sub> reactant valley with the F atom in its ground (<sup>2</sup>P<sub>3/2</sub>) spin-orbit state, is written as

$$\text{eBE} = E - \text{ZPE}(\text{H}_2) + \text{EA}(\text{F}) + D_0(\text{FH}_2^-) \quad (9)$$

where ZPE is the zero-point energy of H<sub>2</sub>, EA is the electron affinity of F, and *D*<sub>0</sub> is the dissociation energy of the FH<sub>2</sub><sup>−</sup> anion, as shown in Figure 2. The value of EA(F) was determined accurately by experimental measurement. The value of ZPE(H<sub>2</sub>) can be determined accurately without much difficulty. However, the dissociation energy *D*<sub>0</sub>(FH<sub>2</sub><sup>−</sup>) is not easy to determine accurately using the state-of-art ab initio method, and currently there is no available experimental value. Therefore, the accuracy of the dissociation energy *D*<sub>0</sub>(FH<sub>2</sub><sup>−</sup>) of the anion PES is very important for accessing the absolute positions of the peaks, which correspond to the transition resonance states in the photodetachment spectra, given by the theoretical simulations.

In the work by Kim et al.,<sup>64</sup> the explicitly correlated coupled-cluster method with single, double, and noniterative triple excitations [CCSD(T)-F12a] and, in addition, the scaled triples correction was applied to calculate the PES of FH<sub>2</sub><sup>−</sup>. In their calculations, an augmented correlation-consistent triple-ζ basis (aug-cc-pVTZ) with a density-fitting basis (JKFIT) tailored for the F12a calculations was used. After solving the vibrational

states of the obtained PES, they found that the dissociation energy *D*<sub>0</sub>(FH<sub>2</sub><sup>−</sup>) is 0.2005 eV.

In general, for a CCSD(T) calculation, the larger the basis set, the higher the accuracy. The calculations of Simons et al. used a triple-ζ basis set; those of Hartke and Werner were somewhat better using a quadruple-ζ basis. Although much larger basis set was applied in the work by Kim et al., the accurate value of *D*<sub>0</sub>(FH<sub>2</sub><sup>−</sup>) remains unclear.

To explore this issue, extensive calculations with high-level ab initio method using large basis set were performed. The convergence of the self-consistent field energy was checked with the aug-cc-pVxZ(x = T/Q/5/6) basis functions and extrapolation method,<sup>77</sup> the coupled cluster theory up to perturbative quadruples was used to investigate the convergence of the electronic correlation energy, and the relativistic effect contribution was checked by the Cowan–Griffin approach<sup>78</sup> and MRCI method<sup>79</sup> implemented in Molpro 2012.1 program.<sup>75</sup> The resulting “most” accurate value of *D*<sub>0</sub>(FH<sub>2</sub><sup>−</sup>) is 0.2028 eV, which should still be of ca. ±1.3 meV (10 cm<sup>−1</sup>) uncertainty. For more details, one may refer to the Supporting Information.

Since the value of ZPE(H<sub>2</sub>) calculated by the CSZ PES is 0.270 26 eV, the final relation between the experimentally measured binding energy of the electron (eBE) and the energy *E* in the theoretical simulation can be written as

$$\begin{aligned} \text{eBE} &= E - E_m = E - 0.270\,26 \text{ eV} + 3.4012 \text{ eV} \\ &+ 0.2028 \text{ eV} = E + 3.3337 \text{ eV} \end{aligned} \quad (10)$$

In the work by Kim et al., *D*<sub>0</sub>(FH<sub>2</sub><sup>−</sup>) = 0.2005 eV was obtained, and along with the experimental values EA(F) = 3.4012 eV and ZPE(H<sub>2</sub>) = 0.2705 eV, they accidentally found that the position of the peak, which corresponds to transition-state resonance (3, 0, 1) (or product resonance (3, 0, 0) in their assignment, vide infra) in the product channel, agreed exactly with the position of the corresponding peak in the experimental spectra. With this observation, they concluded that the LWAL PES is more accurate for reproducing the anion photodetachment spectra of FH<sub>2</sub><sup>−</sup>.

From the discussion above, we know that this criterion may be not a good judgment to access the quality of the PES for F + H<sub>2</sub>, since the accuracy of the state-of-art ab initio method for the value of *D*<sub>0</sub>(FH<sub>2</sub><sup>−</sup>) with uncertainty below ±1 meV is questionable.

**3.3. Electron Photodetachment Spectra of FH<sub>2</sub><sup>−</sup>.** The calculated photodetachment spectra for para- and ortho-FH<sub>2</sub><sup>−</sup> with energy resolution of 1 meV as functions of scattering energy on the CSZ PES, which is measured relative to the classical bottom of the F + H<sub>2</sub> asymptote, are displayed in Figure 3. There are rather rich structures. The overview photodetachment spectrum is dominated by three broad peaks, labeled A, B, and C, for para-FH<sub>2</sub><sup>−</sup> and by four broad peaks, labeled F, G, H, and I, for ortho-FH<sub>2</sub><sup>−</sup>. These had been previously assigned to hindered H<sub>2</sub> rotor (or bending) states of the transient FH<sub>2</sub> complex.<sup>4,53</sup> The equilibrium geometry of the linear FH<sub>2</sub><sup>−</sup> anion is just on the reactant side of the neutral transition state. Because the minimum F + H<sub>2</sub> barrier on the neutral PES has a floppy bent geometry, photodetachment of the electron excites a bending progression with broad peak in the neutral FH<sub>2</sub> complex. Besides the broad peaks, several small sharp peaks α, β, γ, and δ also arise. In this subsection, the dynamics origin of these peaks will be explored using both FF and FTA methods.

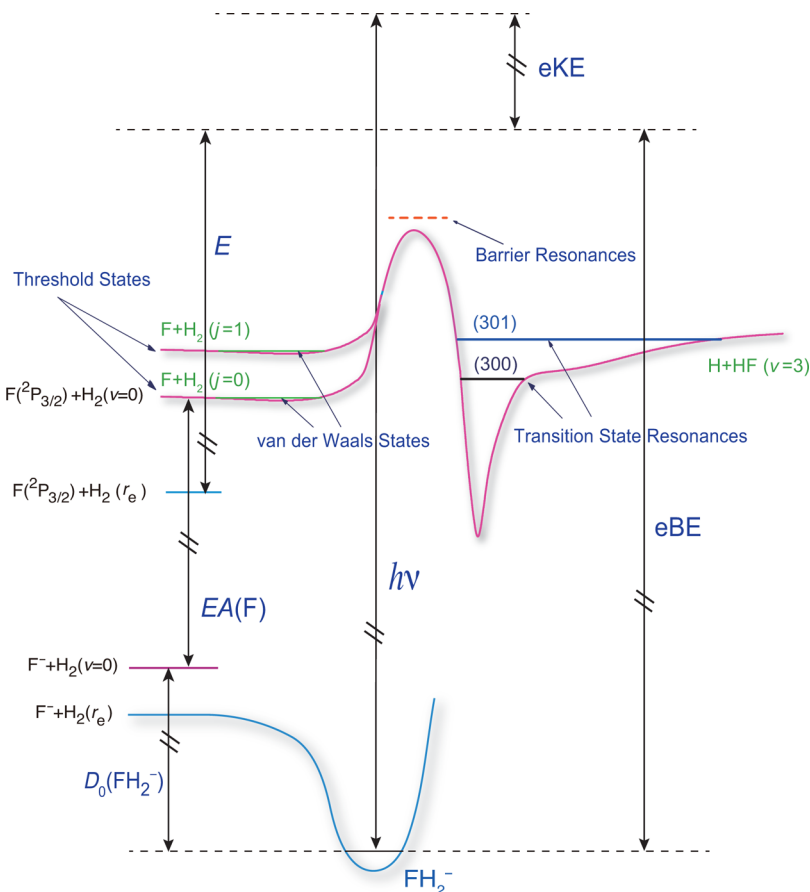


**Figure 2.** Schematic of the energetics of the photodetachment process. Arrows show the relationship between the experimental electron binding energy ( $eBE$ ) and the total scattering energy ( $E$ ) in the calculations. The peaks in the transition spectra can be classified into four classes. (1) van der Waals state. (2) Threshold states. (3) Barrier states. (4) Transition state resonances.

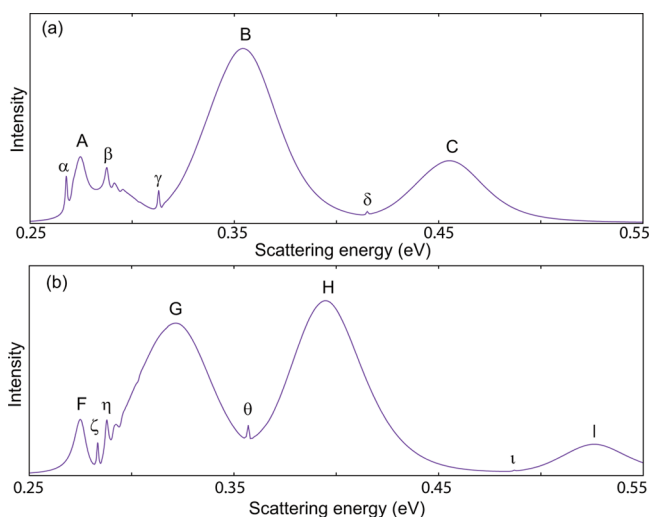


**Figure 3.** High-energy resolution photodetachment spectra of para-FH<sub>2</sub><sup>-</sup> (a) and ortho-FH<sub>2</sub><sup>-</sup> (b) calculated using the FTA method on the CSZ PES for neutral F + H<sub>2</sub>.

First we consider the rather broad peak at  $E = 0.3540$  eV, which appears in the spectrum of para-FH<sub>2</sub><sup>-</sup> labeled as peak B in Figure 3a. The enlarged spectrum around peak B calculated by using the FTA method is presented in Figure 4a along with that using the FF method. Their agreement is excellent, as it should be.

By checking the influence to the calculated results of the value of  $R_L^A$  in the product/reactant asymptote in the FF calculations, it is found that the spectra around the broad peak B is insensitive to the variation of  $R_L^A$ ; thus, peak B is dominated by direct scattering states or states with short lifetimes. The results shown in Figure 4a are the deconvolution of the simulated spectrum into contributions from reactant and product channels, which shows that the broad peak mostly comes from the contribution of the scattering states in the reactant channel. Such decomposition cannot be obtained by using the FTA method.

Because of the sloppy structure of the transition state, clearly peak B is a typical diffuse structure,<sup>80</sup> resulting from the flat PES in the reactant channel experienced by the outgoing F + H<sub>2</sub> fragments along the oscillation in the angular degree of freedom. Figure 4b presents the contribution of the ground vibrational state in the reactant channel and the rotational states distribution. The broad peak at  $E = 0.3540$  eV is dominated by the F + H<sub>2</sub> ( $v = 0, j = 2$ ) scattering state. One may note that the rovibrational energy of F + H<sub>2</sub> (0, 2) is 0.314 eV; therefore, the translational energy of F + H<sub>2</sub> fragments at  $E = 0.354$  eV is rather low, which is only ~41 meV. Thus, the scattering state moves quite slowly and has a very long de Broglie wavelength along the reaction coordinate, which requires an elaborate optimization of the absorbing potential in a long grid range. The time-independent wave function at  $E = 0.3540$  eV, obtained by using the Fourier transformation of the time-dependent wave packet at energy  $E = 0.3540$  eV, is presented in

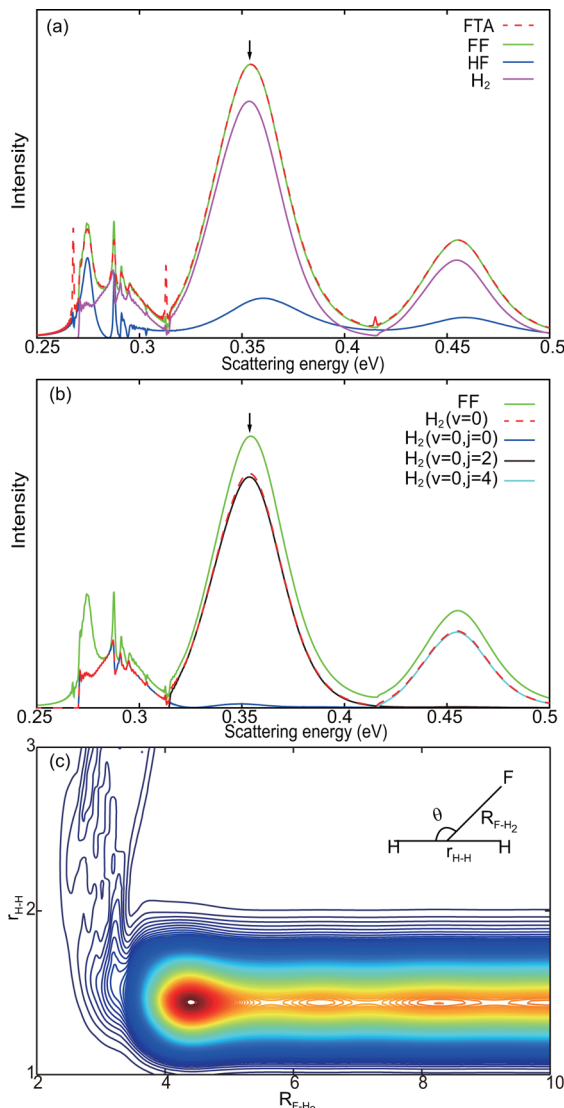


**Figure 4.** (a) The photodetachment spectra of para-FH<sub>2</sub><sup>-</sup> around  $E = 0.3540$  eV (peak B) calculated by using both the FTA and FF method, as well as the contributions from reactant and product channel. (b) The contribution to the photodetachment spectra intensity from rovibrational state of H<sub>2</sub> in the reactant channel. (c) The time-independent wave function at  $E = 0.3540$  eV. All the results are calculated using the CSZ PES for neutral F + H<sub>2</sub>.

Figure 4c. The wave function has a significant distribution over the transition state and in the Franck–Condon region, which illustrates why this scattering state (0, 2) gives rise to a large broad peak in the photodetachment spectra. The peak C in Figure 3a and peaks G, H, and L in Figure 3b have the same dynamics origin as the peak B but with scattering states of quantum number (0, 4), (0, 1), (0, 3), and (0, 5), respectively. These are barrier resonance states, or called quantized bottleneck state.<sup>81,82</sup>

For assigning and understanding resonance states, there are many helpful techniques, other than the time-independent scattering wave function adopted here, such as resonant periodic orbits,<sup>83–86</sup> cumulative reaction probabilities,<sup>87</sup> stabilization method,<sup>88</sup> and vibrationally adiabatic potential curves.<sup>89</sup> The spectral quantization method sometimes is also helpful to assign the quantum number of the resonance states,<sup>81,90,91</sup> especially for states with quite short lifetime.<sup>92</sup> With carefully

designed initial wave function, the wave function around the resonance region would be strengthened, while the direct scattering background could be minimized and thus easier to be identified. Whereas the present straightforward method using the simple but rigorous time-independent wave function works well for understanding the resonance dynamics of F + H<sub>2</sub> and F + HD system, as will be seen in the following, we hesitate to go further with other methods.

Second, we consider the peak at  $E = 0.3129$  eV (peak  $\gamma$ ) in the spectrum of para-FH<sub>2</sub><sup>-</sup>. Figure 5a shows the para-FH<sub>2</sub><sup>-</sup> spectrum calculated via the FTA method, with total integration times between 40 000 and 120 000 a.u. adopted in Fourier transformation. As shown in Figure 5a, the intensity of the sharp peak  $\gamma$  increases continuously with the integration time; in contrast, the intensity of the broader peak at  $E \approx 0.2747$  eV keeps nearly unchanged. This observation indicates that the sharp peak  $\gamma$  is related to a long-lived resonance state, but the broader peak is related to a short-lived one.

To understand further the dynamics of the intermediate states, we performed FF calculations with different locations of  $R_L^i$  where we calculated the flux. Figure 5b, c present the deconvolution of the calculated spectra into rotational state-resolved contributions from reactant and product channels, obtained with  $R_L^i$  located in the product/reactant van der Waals well and asymptote, respectively. As shown in 5b, there is a sharp peak near  $E = 0.3129$  eV appearing on the contributions from the reactant channel but not the product channel, which indicates that the resonance state corresponding to sharp peak resides dominantly in the reactant channel. However, when  $R_L^i$  is moved to a location in the asymptotic region, Figure 5c indicates the peak near  $E = 0.3129$  eV disappears. This interesting phenomenon confirms that the peak near  $E = 0.3129$  eV is dominated by an extremely long-lived state trapped in the van der Waals well of the reactant channel, which is not easy to be obtained by the FF method with full convergence using limited total propagation time.

To assign the quantum numbers of the quasi-bound state, the time-independent wave functions at  $E = 0.3129$  eV are calculated by using Fourier transformation of the time-dependent wave packet (eq 5) and are presented in Figure 5d, e. Since the wave function is nodeless along both the H–H stretch coordinate  $r_{H-H}$  and F – H<sub>2</sub> translational coordinate  $R_{F-H_2}$  but has two nodes along the angular coordinate  $\theta$ , the quantum numbers of this quasi-bound state at peak  $\gamma$  in the reactant van der Waals well can be assigned as  $(v, j, s) = (0, 2, 0)$ , where  $v$ ,  $j$ , and  $s$  represent the H–H stretch quantum number, the H<sub>2</sub> rotational quantum number, and the F–H<sub>2</sub> stretch quantum number, respectively. The peak  $\alpha$  and  $\delta$  in Figure 3a and peak  $\zeta$ ,  $\theta$ , and  $\iota$  in Figure 3b have the same dynamics origin as the peak  $\gamma$  but with scattering states of assignment (0, 0, 0), (0, 4, 0), (0, 1, 0), (0, 3, 0), and (0, 5, 0), respectively.

Finally we consider the two peaks appear at  $E = 0.2750$  (peak F) and 0.2879 eV (peak  $\eta$ ) in the ortho-FH<sub>2</sub><sup>-</sup> photodetachment spectrum. Similarly, Figure 6a presents the calculated spectrum of ortho-FH<sub>2</sub><sup>-</sup> as well as the contributions from the reactant and product channels by the FF method. For energy below  $E = 0.3$  eV, the photodetachment fragments mainly come from the contribution from the product channel. Photodetachment fragments of ortho-FH<sub>2</sub><sup>-</sup> can only lead to F + ortho-H<sub>2</sub> in the reactant channel, and the lowest two accessible final states for the fragments of ortho-FH<sub>2</sub><sup>-</sup> are F + H<sub>2</sub>( $v = 0, j = 1$ ) and F +

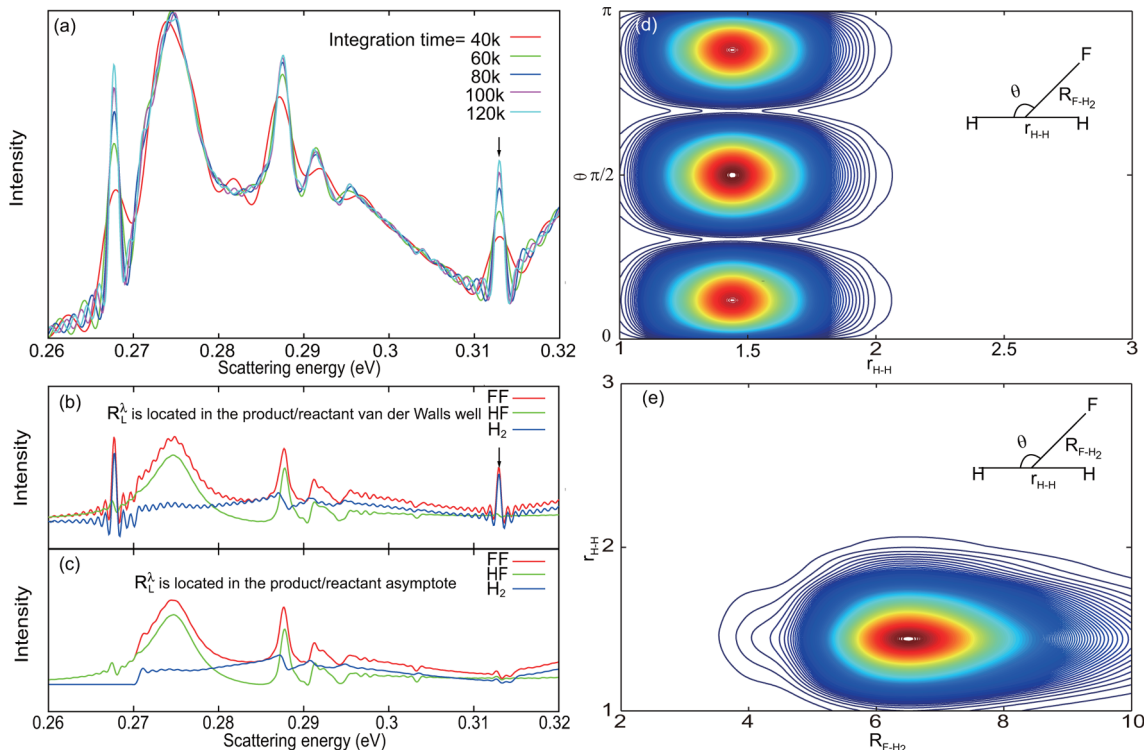


**Figure 5.** (a) The photodetachment spectra of para- $\text{FH}_2^-$  calculated by using the FTA method. Total integration times between 40 000 and 120 000 au are used for the Fourier transformation. (b, c) The same spectrum calculated by using the FF method with  $R_L^\lambda$  located in the product/reactant van der Waals well and asymptotic region. (d, e) The time-independent wave function at  $E = 0.3129$  eV (peak  $\gamma$  indicated by vertical arrow) in reactant Jacobi coordinates, where  $r_{\text{H}-\text{H}}$  has been integrated out. All the results are calculated using the CSZ PES for neutral  $\text{F} + \text{H}_2$ .

$\text{H}_2(\nu = 0, j = 3)$ . Since the threshold energy for opening these two fragments are 0.2849 and 0.3578 eV, another 9.9 meV of energy for the peak at  $E = 0.2750$  eV is required to open the  $\text{F} + \text{H}_2(\nu = 0, j = 1)$  state, and another 69.9 meV of energy for the peak at  $E = 0.2879$  eV to open the  $\text{F} + \text{H}_2(\nu = 0, j = 3)$  channel. This explains why all the photoproducts for resonance state  $E = 0.2750$  (peak F) deposit in the product channel, and only  $\sim 20\%$  of the photoproducts at  $E = 0.2879$  eV deposit in the reactant channel.

In Figure 6b, the vibrational state-resolved contributions of the product channel to the spectrum of ortho- $\text{FH}_2^-$  around peak F and  $\eta$  are presented. These two peaks mainly correlate with the second vibrationally excited state,  $\text{H}+\text{HF}(\nu = 2, j)$ , in the product channel. The contributions of fragments  $\text{H} + \text{HF}(\nu = 2)$  are further decomposed into rotational state-resolved contributions, shown in Figure 6c. The most populated rotational state in the second vibrationally excited state is  $j = 3$ , and each rotational state gives rise to peak F and  $\eta$  with rather close intensities. In contrast, the direct scattering state  $\text{F} + \text{H}_2(\nu = 0, j = 2)$  can only give rise to one broad peak in the spectrum of para- $\text{FH}_2^-$  as illustrated in Figure 4.

To understand the nature of the state at peak F and  $\eta$ , their time-independent wave functions are calculated and presented in Figure 7. The two-dimensional time-independent wave functions in product Jacobi coordinates  $R_{\text{H}-\text{HF}}$  and  $r_{\text{H}-\text{F}}$  are given in Figure 7a for peak F and 7b for peak  $\eta$ , while the angular degree of freedom was integrated out. The panels (c) and (d) of Figure 7 show the same wave functions but in reactant Jacobi coordinates,  $R_{\text{F}-\text{H}_2}$  and  $\theta$ , with integrating out the vibrational coordinate  $r_{\text{H}-\text{H}}$ .

The wave function for peak F in Figure 7a is nodeless along the H–HF stretch coordinate and exhibits three nodes along

the H–F stretch coordinate (related to the HF product), with the outgoing wave function mainly of characteristics of the  $\text{HF}(\nu = 2)$  state. However, the wave function in reactant Jacobi coordinate in Figure 7c accumulates around  $\theta = 20^\circ$  and  $160^\circ$ . Therefore, the state at peak F can be assigned as the  $\text{FH}_2(\nu = 3, j = 0, s = 0)$  reactive resonance localized near the transition state, where  $s$  is the quantum number for the HF–H stretching mode,  $j$  is the quantum number for the bending mode of H–F and H–H bonds, and  $\nu$  is the quantum number for the HF stretching mode. Similarly, the time-independent wave functions in Figure 7b, d can be assigned as the  $\text{FH}_2(\nu = 3, j = 0, s = 1)$  reactive resonance state, as it has one node along the HF–H coordinate. Thus, the two states at peaks F and  $\eta$  are transition-state resonances, which are trapped in the HF–H( $\nu = 3$ ) vibrational adiabatic potential well and decay mostly to produce the  $\text{HF}(\nu = 2)$  product, which explains why the same product state can give rise to two different peaks in the spectrum. The broad peak B in the spectrum is a typical diffuse structure, resulting from periodic motion of floppy angular mode, and thus connects dominantly with one specified rotational state of  $\text{H}_2$ . Recently, the role of transition-state resonance was investigated in the isotope effects in the  $\text{F} + \text{H}_2$  and  $\text{F} + \text{HD} \rightarrow \text{HF} + \text{D}$  reaction; their Figure 3 essentially is same as the wave function in panel (a) of current Figure 7.<sup>33</sup>

The peaks A and  $\beta$  are the same transition resonance states as peaks F and  $\eta$ , respectively. However, since the state at peak A can produce photodetachment fragment  $\text{F} + \text{H}_2(j = 0)$ , in the FF method we must calculate the spectra at peak A in both product and reactant channels, in contrast to peak F, which only decays into the product channel, as shown in Figure 4a.

In the above analysis, we have three different types of peaks/states in the high-resolution photodetachment spectra of  $\text{FH}_2^-$ ,

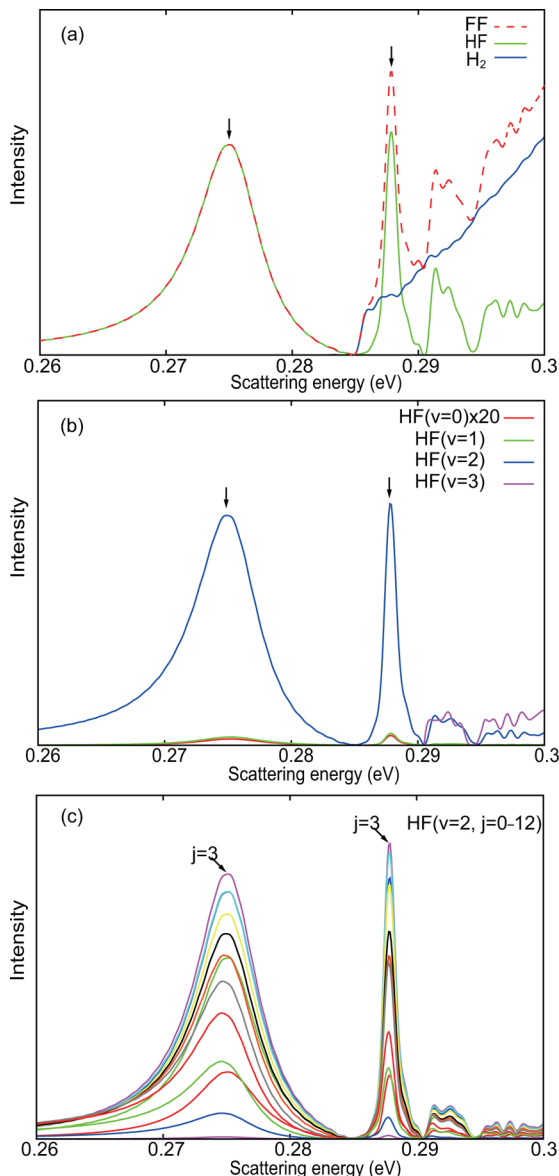


**Figure 6.** (a) The photodetachment spectra of ortho- $\text{FH}_2^-$  and the contributions from the reactant  $\text{F} + \text{H}_2$  and product  $\text{HF} + \text{H}$  channel. (b, c) The rovibrational state-resolved contributions to the spectra in the product channel. All the results are calculated using the CSZ PES for neutral  $\text{F} + \text{H}_2$ .

which were assigned and investigated, including the quasi-bound state trapped in the reactant van der Waals well,  $\text{F}/\text{H}_2(\nu, j, s)$  state, the barrier resonances,  $\text{F} + \text{H}_2(\nu, j)$  state, and the transition-state resonances,  $\text{FH}_2(\nu, j, s)$  state. The last kind of resonance state corresponds to the reactive scattering resonances that received focused studies recently in the crossed molecular beam experiments.<sup>26</sup>

In Table 4 we summarize the assignments for all the peaks with energy less than  $E = 0.6$  eV in the calculated photodetachment spectra of para- and ortho- $\text{FH}_2^-$ . From the data listed in Table 4 and plots in Figure 3, we can find that all the broad peaks result from barrier resonances  $\text{F} + \text{H}_2(\nu = 0, j = 1, 2, 3, 4, 5)$ . It is rather interesting that none of peaks seem to be dominated by the lowest direct scattering state  $\text{F} + \text{H}_2(\nu = 0, j = 0)$ . Actually, that peak overlap with the peak A and  $\beta$ , which cannot be differentiated from each other. Another interesting

observation from Table 4 is that before each broad peak resulting from barrier resonances, there is always a sharp peak resulting from a quasi-bound state trapped in the reactant van der Waals well.

In contrast to the assignment in the work by Kim et al.,<sup>64</sup> we assign the peaks  $\beta$  and  $\eta$  as transition-state resonance  $\text{FH}_2(\nu = 3, j = 0, s = 1)$ , instead of product resonance by Kim et al. (we would prefer the name as van der Waals state in product channel) with quantum number (3, 0, 0) (marked as peak a in Table 1 and Figures 2 and 4 in ref 64). This strengthens the difference between the LWAL and CSZ PES besides the difference between their barrier heights (1.64 vs 1.67 kcal/mol).<sup>25,49</sup> We will see this difference leads to considerable deviation in the differential cross section (DCS) of reactive scattering of  $\text{F} + \text{H}_2$  given the two PESs at energy around transition-state resonances.

In the paper by Skodje et al.,<sup>81,91</sup> the peaks that appear in transition-state spectra are classified into three categories: (1) transition-state resonances, (2) threshold enhancements, and (3) barrier resonances. The first and the third classes investigated in our calculations are typical barrier resonances and transition-state resonances. The threshold resonances do not arise due to the position of the initial state from anion. The van der Waals states did not arise in the work by Skodje et al., due to the features of the PES applied in their study.<sup>42</sup>

**3.4. Comparison with Experimental Observation.** Very recently, Kim et al. reported very high-resolution photodetachment spectra of para- $\text{FH}_2^-$  and para- $\text{FD}_2^-$ .<sup>64</sup> With cooled anion precursors and a high-resolution electron spectrometer, they observed several narrow peaks not seen in previous experiments. Their theoretical calculations, based on a highly accurate LWAL PES for  $\text{F} + \text{H}_2$  reaction, assigned these peaks to resonances associated with quasibound states in the  $\text{HF} + \text{H}$  and  $\text{DF} + \text{D}$  product arrangements and with a quasi-bound state in the transition-state region of the  $\text{F} + \text{H}_2$  reaction. Using the relation in eq 9 with  $D_0(\text{FH}_2^-) = 0.2005$  eV calculated by ab initio method at CCSD(T)-F12a level,<sup>66,67</sup> they found that the position of peak  $\beta$  given by the LWAL PES agrees with the peak in experimental spectra exactly. On the basis of that observation, the authors concluded that the LWAL surface provides a more accurate description of the  $\text{FH}_2$  PES in the region of the product van der Waals well.

As demonstrated by the highly accurate ab initio calculations in Subsection 3.2, the value of  $D_0(\text{FH}_2^-) = 0.2005$  eV given in the work by Kim et al. is never exact. Our value of  $D_0(\text{FH}_2^-)$  given in Subsection 3.2 is 0.2028 eV, calculated with higher level ab initio method and larger basis set, may still have uncertainty of  $\sim 1.3$  meV. With  $D_0(\text{FH}_2^-) = 0.2028$  eV, the anion photodetachment spectra of  $\text{FH}_2^-$  calculated using the CSZ, FXZ, and LWAL PES for neutral  $\text{F} + \text{H}_2$ , are plotted in Figure 8, along with the experimental spectra of high and low resolution taken from ref 64. The potential for calculating ground-state wave function of  $\text{FH}_2^-$  always is taken as the YCS PES.

With  $D_0(\text{FH}_2^-) = 0.2028$  eV, which is only  $\sim 2.3$  meV different from the value given in Kim et al.,<sup>64</sup> none of the neutral surface is capable of giving accurate positions of peaks A and  $\beta$ , as shown in Figure 8a, c, except the FXZ PES. However, we do not think that this suggests the FXZ PES is more accurate, since possibly the good agreement of peak  $\beta$  is accidental and the uncertainty of  $D_0(\text{FH}_2^-) = 0.2028$  eV is ca.  $\pm 1.3$  meV. When the theoretical results are shifted with respect of the position of peak  $\beta$ , that is, shifting the CSZ PES results

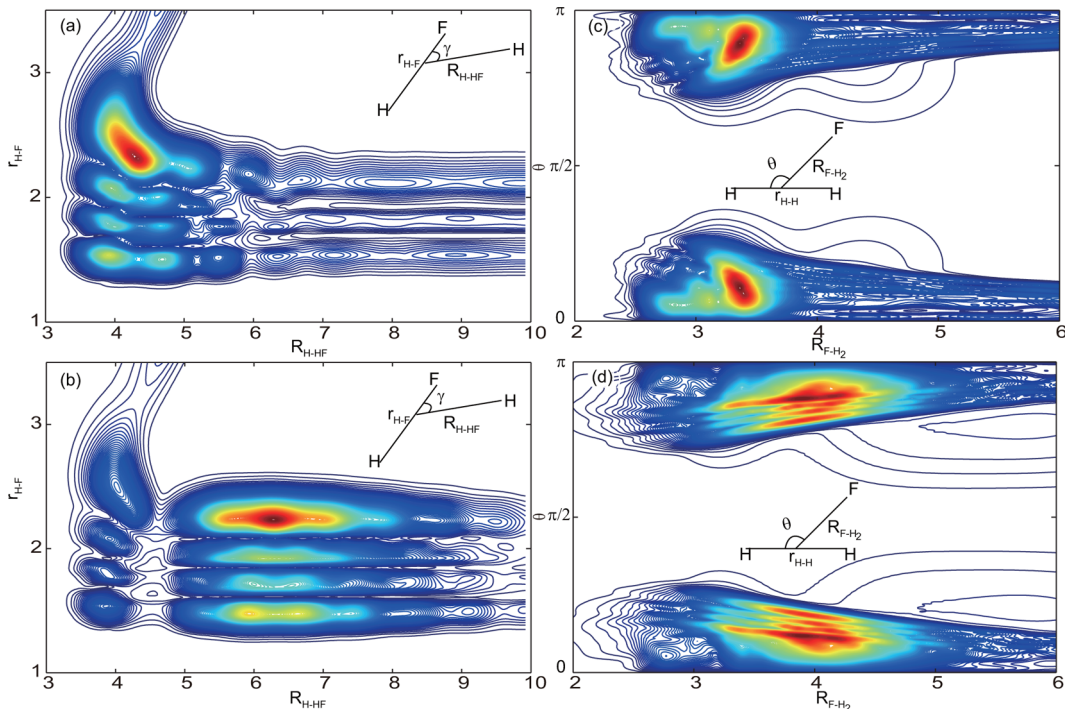


**Figure 7.** Time-independent wave function at  $E = 0.2750$  eV (peak F) in reactant (c) and product (a) Jacobi coordinate. Similarly wave function at  $E = 0.2879$  eV (peak  $\eta$ ) in reactant (d) and product (b) Jacobi coordinate. All the results are calculated using the CSZ PES for neutral  $F + H_2$ .

**Table 4. Assignment of the High-Resolution  $FH_2^-$  Photodetachment Spectra**

| para- $FH_2^-$ |           |                   | ortho- $FH_2^-$ |           |                   |
|----------------|-----------|-------------------|-----------------|-----------|-------------------|
|                | $E$ (meV) | eBE (cm $^{-1}$ ) |                 | $E$ (meV) | eBE (cm $^{-1}$ ) |
| $\alpha$       | 267.7     | 29 042            |                 |           |                   |
| A              | 274.7     | 29 099            | F               | 275.0     | 29 101            |
|                |           |                   | $\zeta$         | 283.4     | 29 169            |
| $\beta$        | 287.6     | 29 203            | $\eta$          | 287.9     | 29 205            |
| $\gamma$       | 312.9     | 29 407            | G               | 321.5     | 29 476            |
| B              | 354.0     | 29 738            |                 |           |                   |
|                |           |                   | $\theta$        | 357.0     | 29 762            |
|                |           |                   | H               | 395.0     | 30 068            |
| $\delta$       | 415.0     | 30 230            |                 |           |                   |
| C              | 455.5     | 30 553            |                 |           |                   |
|                |           |                   | $\iota$         | 487.0     | 30 811            |
|                |           |                   | L               | 526.0     | 31 125            |
|                |           |                   |                 |           |                   |

<sup>a</sup> $F/H_2$  ( $v, j, t$ ),  $F + H_2$  ( $v, j$ ), and  $FH_2$  ( $v, j, t$ ) represent the quasi-bound state in the reactant van der Waals well, the barrier resonances, and the transition resonance states in the HF–H vibrational adiabatic potential well, respectively (see the text).

up 1.5 meV but shifting the LWAL PES results down 2.3 meV, we see that now the agreement between experiment and theoretical spectra is excellent for both the FXZ and CSZ PES. In contrast, the position of the peaks  $\alpha$  and A of the LWAL PES in energy is too low. At the same time, the peak  $\gamma$  of the LWAL PES is narrower than that of the FXZ and CSZ PES and also seems narrower than the experiment, although the exact shape of the photodetachment spectra cannot be simply compared with the current theoretical results using the Franck–Condon approximation, constant transition dipole moment approximation, and  $J_{\text{tot}}$  approximation, since the cross section of

detachment to the reactive neutral  $^2\Sigma$  surface actually is proportional to  $E_{ke}^{1+1/2} = E_{ke}^{3/2}$  according to the Wigner threshold law for photodetachment.<sup>54,93,94</sup> Regardless of this fact, the peaks A and  $\alpha$  given by the FXZ PES are slightly lower than the experiment. In other words, the spacing between peaks A and  $\beta$  given by the CSZ PES agrees best with the experiment among these three PESs. We will see later that such negligible difference detected by the photodetachment spectra can be directly reflected by the comparison between the experimental DCSs of Yang's group and theoretical DCSs using these surfaces. Finally, we emphasize that until now we still do not have definite conclusion as to which PES is the most accurate for describing the dynamics of neutral  $F + H_2$  from the above photodetachment spectra comparison. Anyway, it looks as though the CSZ PES should be the best one currently from the above discussion.

For completeness, the theoretical photodetachment spectra using the neutral CSZ and SW PES are also compared with the experimental spectra of para- $FH_2^-$  of low resolution (~19 meV) reported by Neumark and co-workers in 1993<sup>4</sup> in Figure 9 and with the experimental photodetachment spectra of both normal- $FH_2^-$  of intermediate resolution reported by Neumark and his co-workers in 2012 in Figure 10.<sup>54</sup>

The scattering energy  $E$  is related to the electron kinetic energy eKE and binding energy eBE by an energy conservation relationship that has been discussed in ref 55. The calculated spectra in Figure 9 were energetically shifted according to the experimental measurements, as was done in ref 57. The theoretical spectra on both PESs agree roughly with the experiment. However, quantitatively, there are still some obvious disagreements. The intensity of peak B is too large, and other peaks are too small, as compared with the experiment for both the SW and CSZ PES. As the comparison between the theoretical and experimental results shown in Figure 8, this obvious disagreement should come from the incomplete

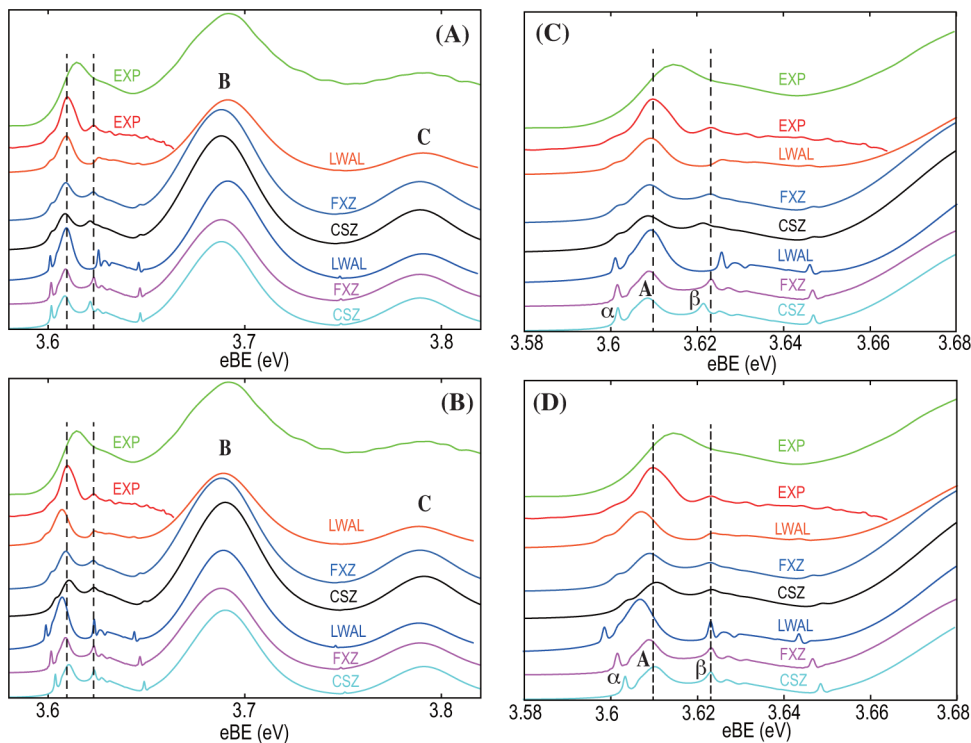


**Figure 8.** High-resolution photodetachment spectra of  $p\text{-FH}_2^-$ . Green: experimental overview spectrum ( $\sim 10$  meV resolution). Purple: highest-resolution experimental spectrum (2 to 3 meV) over a narrower energy window. The experimental results are taken from ref 64. Other lines are the theoretical simulation at 1 meV (lowest three lines) and 3 meV (upper three lines) energy resolution. For the results in panels (A) and (C), the relation between the experimental electron binding energy  $eBE$  and the energy  $E$  relative to  $\text{F}({}^2\text{P}_{3/2}) + \text{H}_2(\text{re})$  is given by eq 10 as  $eBE = E + 3.3338$  eV. However, in panels (B) and (D) the calculated spectra were shifted to match experiment, with respect to the position of peak  $\beta$ .

consideration of the initial states since only the lowest vibrational state of anion and  $J_{\text{tot}} = 0$  were included in the calculation, since the experimental spectra in Figure 9 were not measured in a cooled condition. The relative intensity of peaks A and C is inconsistent with the experiment for the SW PES. In contrast, the calculated spectrum on CSZ PES presents the same trend with experiment. The small shoulder beside peak A (labeled as  $A^*$ ), which arises in the simulated spectra presented in Figure 9b but disappears in the spectra in Figure 9a, comes from the resonance state (3, 0, 1) (peak  $\beta$  in Figure 3) on the CSZ PES. This resonance peak, however, is unobservable in the detachment spectra using the SW PES. This results from the sharp distinction between the SW and CSZ PES around van der Waals region in the product channel.<sup>34</sup>

In the spectra presented in Figure 10, there are some disputations on the assignments of the three peaks arising at  $eBE = 29\ 136$  and  $29\ 180$  cm<sup>-1</sup> in the para- $\text{FH}_2^-$  spectra (labeled as “a” and “b”) and at  $eBE = 29\ 121$  cm<sup>-1</sup> in the ortho- $\text{FH}_2^-$  spectrum (labeled as “x”), as discussed in ref 54. One possible assignment for the three peaks was suggested that peak b might come from the  $\text{F} + \text{H}_2(0, 0)$  direct scattering state, but the peaks a and x would be assigned to the reactive resonance states,<sup>54</sup> which is supported by an earlier analysis of lower-resolution photodetachment spectra.<sup>4</sup> The other possible assignment was that the peak b should come from the convolution of peaks a and c, but peaks a and x result from the  $\text{F} + \text{H}_2(0, 0)$  direct scattering state.<sup>54</sup> From the comparison between the theoretical results and experiments in Figure 10, now it is clear that peak a corresponds to peak A in Figure 3a, peak b is convolution of peaks A and  $\beta$  in Figure 3a, and peak C is peak  $\beta$  in Figure 3a. Thus, all these three peaks a, b, and c

come from transition resonance state of  $\text{FH}_2(v = 3, j = 0, s = 0)$  and  $\text{FH}_2(v = 3, j = 0, s = 1)$ . Peak d is the peak  $\gamma$ , which is a van der Waals state in reactant channel. In the lower panel of Figure 10, the peaks x, y, and z correspond to peaks F,  $\eta$ , and G in Figure 3b, respectively. The former two are transition resonance states, but the last one is a barrier resonance exhibiting diffuse structure.

**3.5. Implications for Resonant Reactive Scattering.** In the past years, extensive studies on the reaction dynamics of  $\text{F} + \text{H}_2$  and its isotopes were performed in Yang’s group with Rydberg tagging crossed molecular beam apparatus. Their high-resolution state-to-state resolved DCSSs have verified that the attributes of reaction  $\text{F} + \text{H}_2/\text{HD}$  given by the CSZ PES agree with the experimental DCSSs at the most detailed state-to-state level with near spectroscopic accuracy. With respect to the difference between the spectra shown in Figure 8 calculated using the neutral LWAL, FXZ, and CSZ PES, and the experiment, it would be helpful to compare and see whether a similar difference of some reactive scattering attributes exists between the results given by these three PESs and crossed molecular beam experiment, to understand in a different way that the experimental results by crossed molecular beam and photodetachment spectra differentiate the best available PESs.

Figure 11a presents the total reaction probabilities of  $\text{F} + \text{H}_2$  ( $v_0 = 0, j_0 = 0$ ) with  $J_{\text{tot}} = 0$ . The peaks, which result from the transition resonance states enhancement, are labeled by the symbols used in Figures 8 and 3. The relative spacings between peaks A and  $\beta$  in Figure 8 exactly are reflected by the spacings between the corresponding peaks in total reaction probabilities shown in Figure 11. Thus, the anion photodetachment spectra can detect the quality of the PES at the level of single partial

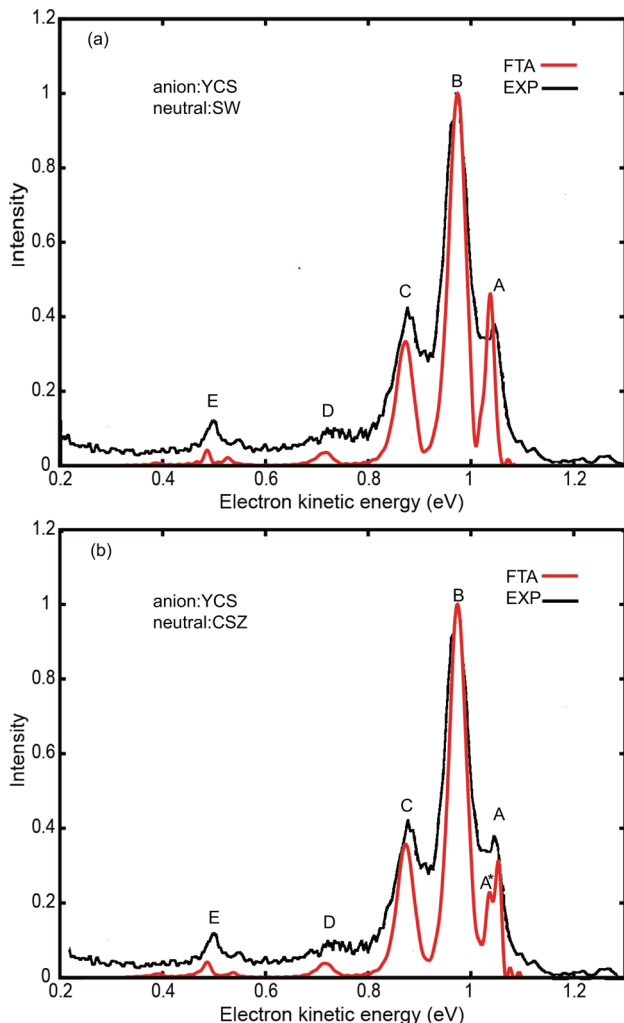


**Figure 9.** A direct comparison between the simulated photodetachment spectra of para- $\text{FH}_2^-$  with the experimental results reported in ref 4, with a low resolution. (a, b) These spectra correspond to quantum dynamics calculations on the SW and CSZ PES for the neutral  $\text{FH}_2$ , respectively.

wave, as expected. Especially, the transition resonance state, which results in narrower peak  $\beta$  in photodetachment spectra on the LWAL PES, leads to similar narrower peak in the total reaction probabilities as a function of collision energy in Figure 11. However, the most interesting transition resonance states, which lead to two strikingly large peaks in the total reaction probabilities, only produce small peaks in the photodetachment spectra since the Franck–Condon region of the ground state of anion resides completely in the reactant channel, far from the resonance region in the product channel. As soon as we have ways to alter the position of the initial state from the anion, such situations can be changed as in the work by Skodje et al.<sup>81</sup>

The DCS is a summation of many partial waves; thus, usually the features of resonance are smeared out. However, the slight difference between the transition resonance state on these three PESs is amplifiedly reflected by the forward scattering as a function of collision energy, as shown in Figure 11b, due to its coherence nature of the summation of the involved partial waves. The slight difference between the spacings of peaks A and  $\beta$  given by the FXZ and CSZ PES bring about distinct positions of the forward scattering peak, that is, peak at lower collision energy by the CSZ PES but peak at higher collision

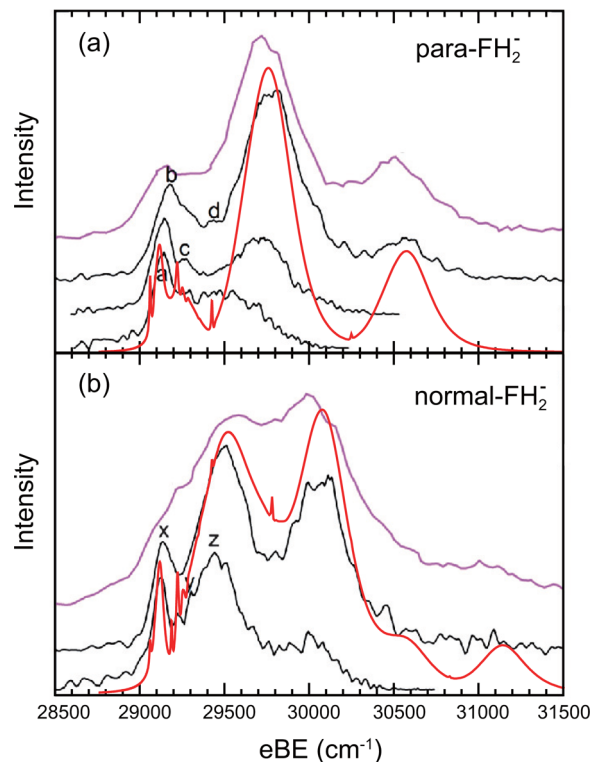


**Figure 10.** Comparison between simulated and experimental spectra of para- and normal- $\text{FH}_2^-$  with intermediate energy resolution. The simulated spectra are shown as red lines. The experimental spectra are taken from ref 54. The experimental spectra are taken at laser energies of 311 nm (upper black traces), 325 nm (next trace), and 329 nm (lower trace, para- $\text{FH}_2^-$  only), and the purple lines correspond to low-energy resolution experimental spectra of ref 4. All the results are calculated using the CSZ PES for neutral  $\text{F} + \text{H}_2$ .

energy by the FXZ PES than the experiment. This forward peak comes from the interference between the transition-state resonance ( $3, 0, 0$ ) (peak A) and ( $3, 0, 1$ ) (peak  $\beta$ ) and thus is sensitive to subtle variation of the characteristics of these two resonance states.<sup>26</sup> As expected, this peak given by the LWAL PES deviates from the experiment much, due to the incorrect energy positions of peak A and  $\beta$ , and too long lifetime of peak  $\beta$ . In this respect, it looks like the forward scattering for the  $\text{F} + \text{H}_2$  reaction for collision energy around the transition resonance state is more sensitive for differentiating the best available PESs.

As we have shown in our recent work,<sup>25</sup> the reaction rate constants of  $\text{F} + \text{HD}$  and  $\text{F} + \text{H}_2$ , the integral cross sections of the two branches of  $\text{F} + \text{HD}$ , backward scattering as a function of collision energy of  $\text{F} + \text{HD}(\nu_0 = 0, j_0 = 0) \rightarrow \text{HF} + \text{D}$ , and the partial wave resonance structure in the  $\text{F} + \text{HD}(\nu_0 = 0, j_0 = 0) \rightarrow \text{HF} + \text{D}$  can be reproduced excellently by the CSZ PES. These combined facts definitely demonstrate that currently the CSZ PES is the best available surface for describing the  $\text{F} + \text{H}_2$  and its isotopes, especially for describing the transition-state resonances in the product channel. This conclusion was also supported by the work by De Fazio et al. where extensive investigations using the FXZ PES were performed for checking its accuracy,<sup>34</sup> as we know that the CSZ PES is the second generation of the FXZ PES by adding more energy points with ab initio method of higher level.<sup>25</sup>

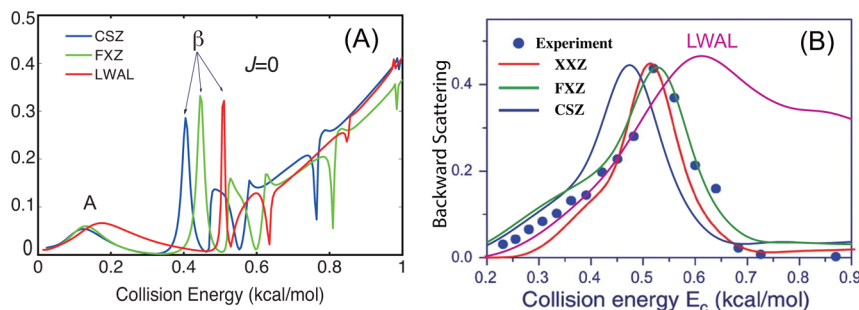


**Figure 11.** (A) Total reaction probabilities calculated using the LWAL, FXZ, and CSZ PES for  $F + H_2$  ( $v_0 = 0, j_0 = 0$ ) reaction. The peaks in the total reaction probabilities clearly correlate with the resonance states A and  $\beta$  in the photodetachment spectra. (B) The forward scattering as a function of collision. The exact agreement of the XXZ PES<sup>26</sup> is an accidental phenomenon. Both the FXZ and CSZ give forward scattering of better agreement with the experiment than that of the LWAL PES.

#### 4. SUMMARY

We have calculated the electron photodetachment spectra of  $FH_2^-$  on highly accurate ab initio SW, FXZ, CSZ, and LWAL PESs for neutral  $F + H_2$  and the YCS PES for anion  $FH_2^-$  constructed in the present work, using Fourier transformation of the autocorrelation function and the flux formalism with time-dependent wavepacket method. The numerical results provide a comprehensive understanding of the photodetachment spectra of  $FH_2^-$ , as well as the transition-state vibrational structure and dynamics for the  $F + H_2$  reaction. The assignments of the peaks appearing in the photodetachment spectra of high resolution of para- and ortho- $FH_2^-$  suggest that all the peaks can be assigned to either one of the quasi-bound states in the reactant channel, the barrier resonance state, or the reactive resonance state localized near the transition state of the  $F + H_2$  reaction. The broad large peaks in the photodetachment spectra come from  $F + H_2$  barrier resonances, which exhibit typical diffuse structures and correspond to threshold state in reactant channel. Before each broad peak arises, there is always a sharp peak dominated by a quasi-bound state trapped in the reactant van der Waals well, which has lower energy than these threshold states. The high-resolution theoretical spectra are compared with the experimental results reported in refs 4, 54, and 64, and excellent agreements are obtained for the FXZ and CSZ PES. Since accurate value of dissociation energy of  $D_0(FH_2^-)$  is not available with the state-of-art ab initio method, the photodetachment spectra are unable to differentiate definitely the quality of the FXZ and CSZ PES. In view of the crossed molecular beam experiment, we reach the conclusion that the best surface among all available PESs is the CSZ PES in the present stage, same as the conclusion arrived at in our previous work.

#### ■ ASSOCIATED CONTENT

##### Supporting Information

The Supporting Information is available free of charge on the ACS Publications website at DOI: [10.1021/acs.jpca.5b06153](https://doi.org/10.1021/acs.jpca.5b06153).

Discussion of investigation of accurate value of dissociation energy  $D_0(FH_2^-)$  using the highest-level ab initio method using large basis set available in the Molpro and NWchem package, tabulated data including SCF energies, correlation energies, post-CCSD(T) contributions, core electron contributions, and relativistic effects. (PDF)

#### ■ AUTHOR INFORMATION

##### Corresponding Authors

\*E-mail: [shlcong@dlut.edu.cn](mailto:shlcong@dlut.edu.cn). (S.C.)

\*E-mail: [zsun@dicp.ac.cn](mailto:zsun@dicp.ac.cn). (Z.S.)

##### Notes

The authors declare no competing financial interest.

#### ■ ACKNOWLEDGMENTS

This work was supported by the National Basic Research Program of China (No. 2013CB922200), the National Natural Science Foundation of China (Grant Nos. 21222308, 21103187, and 21133006), the Chinese Academy of Sciences, and the Key Research Program of the Chinese Academy of Sciences. Z.S. thanks H. Stark and H.-J. Werner for the code of their  $FH_2^-$  potential energy surface and F. Lique and M. H. Alexander for the LWAL potential energy surface.

#### ■ REFERENCES

- (1) Metz, R. B.; Bradforth, S. E.; Neumark, D. M. Transition State Spectroscopy of Bimolecular Reactions Using Negative Ion Photodetachment. *Advances in Chemical Physics* **1991**, *81*, 1–61.
- (2) Neumark, D. M. Transition State Spectroscopy of Bimolecular Chemical Reactions. *Annu. Rev. Phys. Chem.* **1992**, *43*, 153–176.
- (3) Neumark, D. M. Transition-state Spectroscopy via Negative Ion Photodetachment. *Acc. Chem. Res.* **1993**, *26*, 33–40.
- (4) Manolopoulos, D. E.; Stark, K.; Werner, H.-J.; Arnold, D. W.; Bradforth, S. E.; Neumark, D. M. The Transition State of the  $F + H_2$  Reaction. *Science* **1993**, *262*, 1852–1855.
- (5) Alexander, M. H.; Manolopoulos, D. E.; Werner, H.-J. An Investigation of the  $F + H_2$  Reaction Based on a Full Ab Initio Description of the Open-shell Character of the  $F(^2P)$  Atom. *J. Chem. Phys.* **2000**, *113*, 11084–11100.
- (6) Li, G.; Werner, H.-J.; Lique, F.; Alexander, M. H. New Ab Initio Potential Energy Surfaces for the  $F + H_2$  Reaction. *J. Chem. Phys.* **2007**, *127*, 174302–174313.
- (7) Che, L.; Ren, Z. F.; Wang, X. G.; Dong, W. R.; Dai, D. X.; Wang, X. Y.; Zhang, D. H.; Yang, X. M.; et al. Breakdown of the Born-Oppenheimer Approximation in the  $F + o-D_2 \rightarrow DF + D$  Reaction. *Science* **2007**, *317*, 1061–1064.
- (8) Schatz, G. C.; Bowman, J. M.; Kuppermann, A. Large Quantum Effects in the Collinear  $F + H_2 \rightarrow FH + H$  Reaction. *J. Chem. Phys.* **1973**, *58*, 4023–4025.
- (9) Schatz, G. C.; Bowman, J. M.; Kuppermann, A. Exact quantum, Quasiclassical, and Semiclassical Reaction Probabilities for the Collinear  $F + H_2 \rightarrow FH + H$  Reaction. *J. Chem. Phys.* **1975**, *63*, 674–684.
- (10) Wu, S. F.; Johnson, B. R., III; Levine, R. D. Collinear ABC Reaction with Some Model Potential Energy Surfaces. *Mol. Phys.* **1973**, *25*, 839–856.

- (11) Neumark, D. M.; Wodtke, A. M.; Robinson, G. N.; Hayden, C. C.; Lee, Y. T. Experimental Investigation of Resonances in Reactive Scattering: The F + H<sub>2</sub> Reaction. *Phys. Rev. Lett.* **1984**, *53*, 226–229.
- (12) Neumark, D. M.; Wodtke, A. M.; Robinson, G. N.; Hayden, C. C.; Lee, Y. T. Molecular Beam Studies of the F + H<sub>2</sub> Reaction. *J. Chem. Phys.* **1985**, *82*, 3045–3066.
- (13) Neumark, D. M.; Wodtke, A. M.; Robinson, G. N.; Hayden, C. C.; Shobatake, K.; Sparks, R. K.; Schafer, T. P.; Lee, Y. T. Molecular Beam Studies of the F + D<sub>2</sub> and F + HD Reactions. *J. Chem. Phys.* **1985**, *82*, 3067–3077.
- (14) Aoiz, F. J.; Bañares, L.; Herrero, V. J.; Saez Rabanos, V.; Stark, K.; Werner, H. Classical Dynamics for the F + H<sub>2</sub> → HF + H Reaction on a New Ab Initio Potential Energy surface: A Direct Comparison with Experiment. *Chem. Phys. Lett.* **1994**, *223*, 215–226.
- (15) Evans, M. G.; Polanyi, M. Some Applications of the Transition State Method to the Calculation of Reaction Velocities, Especially in Solution. *Trans. Faraday Soc.* **1935**, *31*, 875–894.
- (16) Castillo, J.-F.; Manolopoulos, D. E.; Stark, K.; Werner, H.-J. Quantum Mechanical Angular Distributions for the F + H<sub>2</sub> Reaction. *J. Chem. Phys.* **1996**, *104*, 6531–6546.
- (17) Skodje, R. T.; Skouteris, D.; Manolopoulos, D. E.; Lee, S.-H.; Dong, F.; Liu, K. Resonance-Mediated Chemical Reaction: F + HD → HF + D. *Phys. Rev. Lett.* **2000**, *85*, 1206–1209.
- (18) Skodje, R. T.; Skouteris, D.; Manolopoulos, D. E.; Lee, S.-H.; Dong, F.; Liu, K. Observation of a Transition State Resonance in the Integral Cross Section of the F+HD Reaction. *J. Chem. Phys.* **2000**, *112*, 4536–4552.
- (19) Liu, K. In *Advances in Chemical Physics*; Rice, S., Dinner, A., Eds.; 2012; Vol. 149, pp 1–46.
- (20) Skodje, R. T. Resonances in Bimolecular Chemical Reactions. *Adv. Quantum Chem.* **2012**, *63*, 119–163.
- (21) Lee, S.-H.; Dong, F.; Liu, K. Reaction Dynamics of F + HD → HF + D at Low Energies: Resonant Tunneling Mechanism. *J. Chem. Phys.* **2002**, *116*, 7839–7848.
- (22) Dong, F.; Lee, S.-H.; Liu, K. Reactive Excitation Functions for F + p-H<sub>2</sub>/n-H<sub>2</sub>/D<sub>2</sub> and the Vibrational Branching for F + HD. *J. Chem. Phys.* **2000**, *113*, 3633–3640.
- (23) Xu, C. X.; Xie, D. Q.; Zhang, D. H. A Global ab initio Potential Energy Surface for F+H<sub>2</sub> → HF+H. *Huaxue Wuli Xuebao* **2006**, *19*, 96–98.
- (24) Fu, B. F.; Xu, X.; Zhang, D. H. A Hierarchical Construction Scheme for Accurate Potential Energy Surface Generation: An Application to the F + H<sub>2</sub> Reaction. *J. Chem. Phys.* **2008**, *129*, 011103–011106.
- (25) Chen, J.; Sun, Z.; Zhang, D. H. An Accurate Potential Energy Surface for the F + H<sub>2</sub> → HF + H Reaction by the Coupled-Cluster Method. *J. Chem. Phys.* **2015**, *142*, 024303–024313.
- (26) Qiu, M.; Ren, Z.; Che, L.; Dai, D.; Harich, S. A.; Wang, X.; Yang, X. Observation of Feshbach Resonances in the F + H<sub>2</sub> → HF + H Reaction. *Science* **2006**, *311*, 1440–1443.
- (27) Ren, Z. F.; Che, L.; Qiu, M. H.; Wang, X. A.; Dai, D. X.; Harich, S. A.; Wang, X. Y.; Yang, X. M.; Xu, C. X.; et al. Probing Feshbach Resonances in F + H<sub>2</sub>(*j* = 1) → HF + H: Dynamical Effect of Single Quantum H<sub>2</sub>-Rotation. *J. Chem. Phys.* **2006**, *125*, 151102.
- (28) Yang, X. M. State-to-State Dynamics of Elementary Bimolecular Reactions. *Annu. Rev. Phys. Chem.* **2007**, *58*, 433–459.
- (29) Ren, Z. F.; Che, L.; Qiu, M. H.; Wang, X. A.; Dong, W. R.; Dai, D. X.; Wang, X. Y.; Yang, X. M.; Sun, Z. G.; et al. Probing the Resonance Potential in the F Atom Reaction with Hydrogen Deuteride with Spectroscopic Accuracy. *Proc. Natl. Acad. Sci. U. S. A.* **2008**, *105*, 12662–12666.
- (30) Wang, X.; Dong, W.; Qiu, M.; Ren, Z.; Che, L.; Dai, D.; Wang, X.; Yang, X.; Sun, Z.; et al. HF(*v'* = 3) Forward Scattering in the F + H<sub>2</sub> Reaction: Shape Resonance and Slow-down Mechanism. *Proc. Natl. Acad. Sci. U. S. A.* **2008**, *105*, 6227–6231.
- (31) Dong, W. R.; Xiao, C. L.; Wang, T.; Dai, D. X.; Yang, X. M.; Zhang, D. H. Transition-State Spectroscopy of Partial Wave Resonances in the F + HD Reaction. *Science* **2010**, *327*, 1501–1502.
- (32) Yang, X.; Zhang, D. H. Dynamical Resonances in the Fluorine Atom Research with the Hydrogen Molecule. *Acc. Chem. Res.* **2008**, *41*, 981–989.
- (33) Wang, T.; Yang, T. G.; Xiao, C. L.; Sun, Z. G.; Huang, L.; Dai, D. X.; Yang, X. M.; Zhang, D. H. Isotope-Dependent Rotational States Distributions Enhanced by Dynamic Resonance States: A Comparison Study of the F + HD → HF(*v<sub>HF</sub>* = 2) + D and F + H<sub>2</sub> → HF(*v<sub>HF</sub>* = 2) + H Reaction. *J. Phys. Chem. Lett.* **2014**, *5*, 3049–3055.
- (34) De Fazio, D.; Lucas, J. M.; Aquilanti, V.; Cavalli, S. Exploring the Accuracy Level of New Potential Energy Surfaces for the F + HD Reactions: from Exact Quantum Rate Constants to the State-to-State Reaction Dynamics. *Phys. Chem. Chem. Phys.* **2011**, *13*, 8571.
- (35) Werner, H.; Kállay, M.; Gauss, J. The Barrier Height of the F + H<sub>2</sub> Reaction Revisited: Coupled-cluster and Multireference Configuration-interaction Benchmark Calculations. *J. Chem. Phys.* **2008**, *128*, 034305.
- (36) Tizniti, M.; Le Picard, S. D.; Lique, F.; Berteloot, C.; Canosa, A.; Alexander, M. H.; Sims, I. R. The Rate of the F + H<sub>2</sub> Reaction at very Low Temperatures. *Nat. Chem.* **2014**, *6*, 141–145.
- (37) De Fazio, D.; Cavalli, S.; Aquilanti, V.; Buchachenko, A. A.; Tscherbul, T. V. On the Role of Scattering Resonances in the F + HD Reaction Dynamics. *J. Phys. Chem. A* **2007**, *111*, 12538.
- (38) Aquilanti, V.; Cavalli, S.; De Fazio, D.; Simoni, A.; Tscherbul, T. V. Direct Evaluation of the Lifetime Matrix by the Hyperquantization Algorithm: Narrow Resonances in the F + H<sub>2</sub> Reaction Dynamics and Their Splitting for Bonzero Angular Momentum. *J. Chem. Phys.* **2005**, *123*, 054314.
- (39) Aquilanti, V.; Cavalli, S.; Simoni, A.; Aguilar, A.; Lucas, J. M.; De Fazio, D. Lifetime of Reactive Scattering Resonances: Q-matrix Analysis and Angular Momentum Dependence for the F + H<sub>2</sub> Reaction by the Hyperquantization Algorithm. *J. Chem. Phys.* **2004**, *121*, 11675.
- (40) Sokolovski, D.; Sen, S. K.; Aquilanti, V.; Cavalli, S.; De Fazio, D. Interacting Resonances in the F + H<sub>2</sub> Reaction Revisited: Complex Terms, Riemann Surfaces, and Angular Distributions. *J. Chem. Phys.* **2007**, *126*, 084305.
- (41) Sokolovski, D.; Castillo, J. F.; Tully, C. Semiclassical Angular Scattering in the F + H<sub>2</sub> → HF + H Reaction: Regge Pole Analysis Using the Páde Approximation. *Chem. Phys. Lett.* **1999**, *313*, 225–234.
- (42) Takayanagi, T.; Kurosaki, Y. Avan der Waals Resonances in Cumulative Reaction Probabilities for the F + H<sub>2</sub>, D<sub>2</sub>, and HD Reactions. *J. Chem. Phys.* **1998**, *109*, 8929–8934.
- (43) Aoiz, F. J.; Bañares, L.; Herrero, V. J.; Sáez Rábano, V.; Stark, K.; Werner, H. J. The F+HD → DF(HF) + H(D) Reaction Revisited: Quasiclassical Trajectory Study on an Ab Initio Potential Energy Surface and Comparison with Molecular Beam Experiments. *J. Chem. Phys.* **1995**, *102*, 9248–9262.
- (44) Johnston, G. W.; Kornweitz, H.; Schechter, I.; Persky, A.; Katz, B.; Bersohn, R.; Levine, R. D. The Branching Ratio in the F+HD Reaction: An Experimental and Computational Study. *J. Chem. Phys.* **1991**, *94*, 2749–2757.
- (45) Song, J.; Gislason, E. A. Theoretical Study of the Intramolecular Isotope Effect in the Reaction of F + HD. *J. Chem. Phys.* **1996**, *104*, 5834–5844.
- (46) Skouteris, D.; De Fazio, D.; Cavalli, S.; Aquilanti, V. Quantum Stereodynamics for the Two Product Channels of the F + HD Reaction From the Complete Scattering Matrix in the Stereodirected Representation. *J. Phys. Chem. A* **2009**, *113*, 14807–14812.
- (47) De Fazio, D.; Aquilanti, V.; Cavalli, S.; Aguilar, A.; Lucas, J. M. Exact State-to-State Quantum Dynamics of the F + HD → HF(*v'* = 2) + D Reaction on Model Potential Energy Surfaces. *J. Chem. Phys.* **2008**, *129*, 064303.
- (48) Cavalli, S.; Aquilanti, V.; Mundim, K. C.; De Fazio, D. Theoretical Reaction Kinetics Astride the Transition between Moderate and Deep Tunneling Regimes: The F + HD Case. *J. Phys. Chem. A* **2014**, *118*, 6632–6641.
- (49) Lique, F.; Li, G.; Werner, H.-J.; Alexander, M. H. Non-adiabatic Coupling and Resonances in the F + H<sub>2</sub> Reaction at Low Energies. *J. Chem. Phys.* **2011**, *134*, 231101.

- (50) Wang, T.; Chen, J.; Yang, T.; Xiao, C.; Sun, Z.; Huang, L.; Dai, D.; Yang, X.; Zhang, D. H. Dynamical Resonances Accessible Only by Reagent Vibrational Excitation in the  $F + HD \rightarrow HF + D$  Reaction. *Science* **2013**, *342*, 1499–1502.
- (51) Weaver, A.; Metz, R. B.; Bradford, S. E.; Neumark, D. M. Investigation of the  $F + H_2$  Transition State Region via Photoelectron Spectroscopy of the  $FH_2^-$  Anion. *J. Chem. Phys.* **1990**, *93*, 5352–5353.
- (52) Weaver, A.; Neumark, D. M. Negative-ion Photodetachment as a Probe of Bimolecular Transition States: the  $F + H_2$  Reaction. *Faraday Discuss. Chem. Soc.* **1991**, *91*, 5–16.
- (53) Bradford, S. E.; Arnold, D. W.; Neumark, D. M.; Manolopoulos, D. E. Experimental and Theoretical Studies of the  $F + H_2$  Transition State Region via Photoelectron Spectroscopy of  $FH_2^-$ . *J. Chem. Phys.* **1993**, *99*, 6345–6359.
- (54) Yacovitch, T. I.; Garand, E.; Kim, J. B.; Hock, C.; Theis, T.; Neumark, D. M. vibrationally Resolved Transition State Spectroscopy of the  $F + H_2$  and  $F + CH_4$  Reactions. *Faraday Discuss.* **2012**, *157*, 399–414.
- (55) Zhang, J. Z. H.; Miller, W. H. Photodissociation and Continuum Resonance Raman Cross Sections and General Franck-Condon Intensities from S-matrix Kohn Scattering Calculations with Application to the Photoelectron Spectrum of  $H_2F^+ + h\nu \rightarrow H_2F + HF + H + e^-$ . *J. Chem. Phys.* **1990**, *92*, 1811–1818.
- (56) Zhang, J. Z. H.; Miller, W. H.; Weaver, A.; Neumark, D. M. Quantum Reactive Scattering Calculations of Franck-Condon Factors for the Photodetachment of  $H_2F^-$  and  $D_2F^-$  Comparisons with Experiment. *Chem. Phys. Lett.* **1991**, *182*, 283–289.
- (57) Russell, C. L.; Manolopoulos, D. E. How to Observe the Elusive Resonances in  $F + H_2$  Reactive Scattering. *Chem. Phys. Lett.* **1996**, *256*, 465–473.
- (58) Hartke, B.; Werner, H.-J. Time-dependent Quantum Simulations of  $FH_2^-$  Photoelectron Spectra on New Ab Initio Potential Energy Surfaces for the Anionic and the Neutral Species. *Chem. Phys. Lett.* **1997**, *280*, 430–438.
- (59) Steckler, R.; Truhlar, D. G.; Garrett, B. C. Variational Transition State Theory Calculations of the Reaction Rates of F with  $H_2$ ,  $D_2$ , and  $HD$  and the Intermolecular and Intramolecular Kinetic Isotope Effects. *J. Chem. Phys.* **1985**, *82*, 5499–5505.
- (60) Muckerman, J. T. Applications of Classical Trajectory Techniques to Reactive Scattering. *Theor. Chem. Adv. Perspect. A* **1981**, *6*, 1–77.
- (61) Takayanagi, T.; Sato, S. A Modified LEPS Potential Energy Surface for the  $F + H_2$  Reaction. *Chem. Phys. Lett.* **1988**, *144*, 191–193.
- (62) Lynch, G.; Steckler, R.; Schwenke, D. W.; Varandas, A. J. C.; Truhlar, D. G.; Garrett, B. C. Use of Scaled External Correlation, a Double Many-body Expansion, and Variational Transition State Theory to Calibrate a Potential Energy Surface for  $FH_2$ . *J. Chem. Phys.* **1991**, *94*, 7136–7149.
- (63) Stark, K.; Werner, H.-J. An Accurate Multireference Configuration Interaction Calculation of the Potential Energy Surface for the  $F + H_2 \rightarrow HF + H$  Reaction. *J. Chem. Phys.* **1996**, *104*, 6515–6530.
- (64) Kim, J. B.; Weichman, M. L.; Sjolander, T. F.; Neumark, D. M.; Klos, J.; Alexander, M. H.; Manolopoulos, D. E. Spectroscopic Observation of Resonances in the  $F + H_2$  Reaction. *Science* **2015**, *349*, 510–513.
- (65) Blondel, C.; Delsart, C.; Goldfarb, F. Electron Spectrometry at the  $\mu$ eV Level and the Electron Affinities of Si and F. *J. Phys. B: At., Mol. Opt. Phys.* **2001**, *34*, L281–L288.
- (66) Adler, T. B.; Knizia, G.; Werner, H. A Simple and Efficient CCSD(T)-F12 Approximation. *J. Chem. Phys.* **2007**, *127*, 221106.
- (67) Knizia, G.; Adler, T. B.; Werner, H. Simplified CCSD(T)-F12 Methods: Theory and Benchmarks. *J. Chem. Phys.* **2009**, *130*, 054104.
- (68) Schatz, G. C. Quantum Theory of Photodetachment Spectra of Transition States. *J. Phys. Chem.* **1990**, *94*, 6157–6164.
- (69) Schatz, G. C. A. Three Dimensional Reactive Scattering Study of the Photodetachment Spectrum of  $ClHCl^-$ . *J. Chem. Phys.* **1989**, *90*, 3582–3589.
- (70) Zhang, D. H.; Yang, M.; Collins, M. A.; Lee, S.-Y. Probing the Transition state via Photoelectron and Photodetachment Spectroscopy of  $H_3O^-$ . *Proc. Natl. Acad. Sci. U. S. A.* **2002**, *99*, 11579–11582.
- (71) Zhang, D. H.; Zhang, J. Z. H. Quantum Reactive Scattering with a Deep Well: Time-dependent Calculation for  $H + O_2$  Reaction and Bound State Characterization for  $HO_2$ . *J. Chem. Phys.* **1994**, *101*, 3671–3678.
- (72) Light, J. C.; Hamilton, I. P.; Lill, J. V. Generalized Discrete Variable Approximation in Quantum Mechanics. *J. Chem. Phys.* **1985**, *82*, 1400–1409.
- (73) Sun, Z. G.; Lee, S. Y.; Guo, H.; Zhang, D. H. Comparison of Second-order Split Operator and Chebyshev Propagator in Wave Packet Based State-to-state Reactive Scattering Calculations. *J. Chem. Phys.* **2009**, *130*, 174102–174112.
- (74) Nichols, J. A.; Kendall, R. A.; Cole, S. J.; Simons, J. Theoretical Study of Anion-Molecule Interactions:  $H^- + HF \rightarrow H_2 + F^-$ . *J. Phys. Chem.* **1991**, *95*, 1074–1076.
- (75) Werner, H.; Knowles, P. J.; Knizia, G.; Manby, F. R.; Schütz, M.; et al. *MOLPRO version 2012.1, a package of ab initio programs*, 2012.
- (76) Hagan, M. T.; Menhaj, M. B. Training Feedforward Networks with the Marquardt Algorithm. *IEEE Trans. Neural Net.* **1994**, *5*, 989–993.
- (77) Halkier, A.; Helgaker, T.; Jørgensen, P.; Klopper, W.; Koch, H.; Olsen, J.; Wilson, A. K. Basis-set Convergence in Correlated Calculations on Ne, N<sub>2</sub>, and H<sub>2</sub>O. *Chem. Phys. Lett.* **1998**, *286*, 243–252.
- (78) Martin, R. L. All-electron Relativistic Calculations on Silver Hydride. An Investigation of the Cowan-Griffin Operator in a Molecular Species. *J. Phys. Chem.* **1983**, *87*, 750–754.
- (79) Werner, H.; Knowles, P. J. An Efficient Internally Contracted Multiconfiguration Reference Configuration Interaction Method. *J. Chem. Phys.* **1988**, *89*, 5803–5814.
- (80) Schinke, R. *Photodissociation Dynamics*; Cambridge University Press: New York, 1993.
- (81) Skodje, R. T.; Sadeghi, R.; Krause, J. L. Quantum Dynamics at the Transition State Spectral Quantization and Spectral Control Theory Applied to the  $FH_2^-$  Photodetachment Process. *J. Chem. Soc., Faraday Trans.* **1997**, *93*, 765–772.
- (82) Skodje, R. T.; Yang, X. M. The Observation of Quantum Bottleneck States. *Int. Rev. Phys. Chem.* **2004**, *23*, 253–287.
- (83) Hahn, O.; Taylor, H. S. A Classical Mechanical Analysis of Molecular Motions: Resonances in Transition? state spectra of  $FH_2^-$ ,  $FDH^+$ , and  $FD_2^-$ . *J. Chem. Phys.* **1992**, *96*, 5915–5923.
- (84) Gomez Llorente, J. M.; Pollak, E. Classical Dynamics Methods for High Energy Vibrational Sepctroscopy. *Annu. Rev. Phys. Chem.* **1992**, *43*, 91–126.
- (85) Pollak, E.; Child, M. S. A Simple Classical Prediction of Quantal Resonances in Collinear Reactive Scattering. *Chem. Phys.* **1981**, *60*, 23–32.
- (86) Pollak, E. A Classical Determination of vibrationally Adiabatic Barriers and Wells of a Collinear Potential Energy Surface. *J. Chem. Phys.* **1981**, *74*, 5586–5594.
- (87) Kress, J. D.; Hayes, D. E. Assignment of Peaks in Photodetachment Spectra Using Predicted Densities of Reactive States: Application to  $H_2F^-$  and  $D_2F^-$ . *J. Chem. Phys.* **1992**, *97*, 4881–4889.
- (88) Thompson, T. C.; Truhlar, D. G. Stabilization Calculations and Probability Densities for the Well-Studied Collisional Resonances in Collinear  $F + H_2$ ,  $F + HD$ , and  $F + D_2$ . *J. Phys. Chem.* **1984**, *88*, 210–214.
- (89) Hayes, E. F.; Walker, R. B. Theoretical Analysis of the Reaction  $F + H_2 (v = 0) \rightarrow HF (V = 0, 1, 2, 3)$ . *J. Phys. Chem.* **1982**, *86*, 85–91.
- (90) Skodje, R. T.; Köppel, H.; Sadeghi, R.; Krause, J. L. Spectral Quantization of Transition State Dynamics for the Three Dimensional  $H + H_2$  Reaction. *J. Chem. Phys.* **1994**, *101*, 1725–1729.
- (91) Sadeghi, R.; Skodje, R. T. Barriers, Thresholds, and Resonances: Spectral Quantization of the Transition State for the Collinear  $D + H_2$  Reaction. *J. Chem. Phys.* **1995**, *102*, 193–213.

- (92) Yang, T. G.; Chen, J.; Huang, L.; Wang, T.; Xiao, C. L.; Sun, Z. G.; Dai, D. X.; Yang, X. M.; Zhang, D. H. Extremely Short-Lived Reaction Resonances in Cl + HD( $v = 1$ ) → DCl + H due to Chemical Bond Softening. *Science* **2015**, 347, 60–63.
- (93) Wigner, E. P. On the Behaviour of Cross Sections Near Thresholds. *Phys. Rev.* **1948**, 73, 1002–1009.
- (94) Bartels, C.; Hock, C.; Huwer, J.; Kuhnen, R.; Schwöbel, J.; von Issendorff, B. Probing the Angular Momentum Character of the Valence Orbitals of Free Sodium Nanoclusters. *Science* **2009**, 323, 1323–1327.